A Study of Optimal Membrane Triangles with Drilling Freedoms

C. A. Felippa

Publication CIMNE Nº-218, September 2002

A Study of Optimal Membrane Triangles with Drilling Freedoms

C.A. Felippa

Publication CIMNE Nº-218, September 2002

International Center for Numerical Methods in Engineering
Gran Capitán s/n, 08034 Barcelona, Spain

TABLE OF CONTENTS

A Study of Optimal Membrane Triangles with Drilling Freedoms

CARLOS A. FELIPPA

Department of Aerospace Engineering Sciences and
Center for Aerospace Structures
University of Colorado
Boulder, Colorado 80309-0429, USA

SUMMARY

This article compares derivation methods for constructing optimal membrane triangles with corner drilling freedoms. The term "optimal" is used in the sense of exact inplane pure-bending response of rectangular mesh units of arbitrary aspect ratio. Following a comparative summary of element formulation approaches, the construction of an optimal 3-node triangle using the ANDES formulation is presented. The construction is based upon techniques developed by 1991 in student term projects, but taking advantage of the more general framework of templates developed since. The optimal element that fits the ANDES template is shown to be unique if energy orthogonality constraints are enforced *a priori*. Two other formulations are examined and compared with the optimal model. Retrofitting the conventional LST (Linear Strain Triangle) element by midpoint-migrating by congruential transformations is shown to be unable to produce an optimal element while rank deficiency is inevitable. Use of the quadratic strain field of the 1988 Allman triangle, or linear filtered versions thereof, is also unable to reproduce the optimal element. Moreover these elements exibit serious aspect ratio lock. These predictions are verified on benchmark examples.

Keywords: finite elements, templates, high performance, drilling freedoms, triangles, membrane, plane stress, shell, assumed natural deviatoric strains, hierarchical models, signatures, clones.

1. INTRODUCTION

One active area of "finitelementology" is the development of high-performance (HP) elements. The definition of such creatures is subjective. The writer likes to use a result-oriented definition, as stated in [1]: "simple elements that provide results of engineering accuracy with coarse meshes."

But what are "simple" elements? Again that term is subjective. The writer's definition is: *elements with only corner nodes and physical degrees of freedom.* Following the high-order element frenzy of the late 1960s and 1970s, the back trend towards simplicity was noted as early as 1986 by the father of NASTRAN: "The limitations of higher order elements set out by Zienkiewicz have proved themselves in application. As a practical matter, the real choice is between lowest order elements (constant strain, probably with some linear strain terms) and next-lowest-order elements (linear strain, possibly with some quadratic strain terms), because these are the ones that developers of finite element programs have found to be commercially viable" [2, p. 89].

The trend has strenghtened since that statement because commercial FEM codes are now used by comparatively more novices, often as backend of CAD studies. These users have at best only a foggy notion of what goes on inside the black boxes. Hence the writer's admonition in an

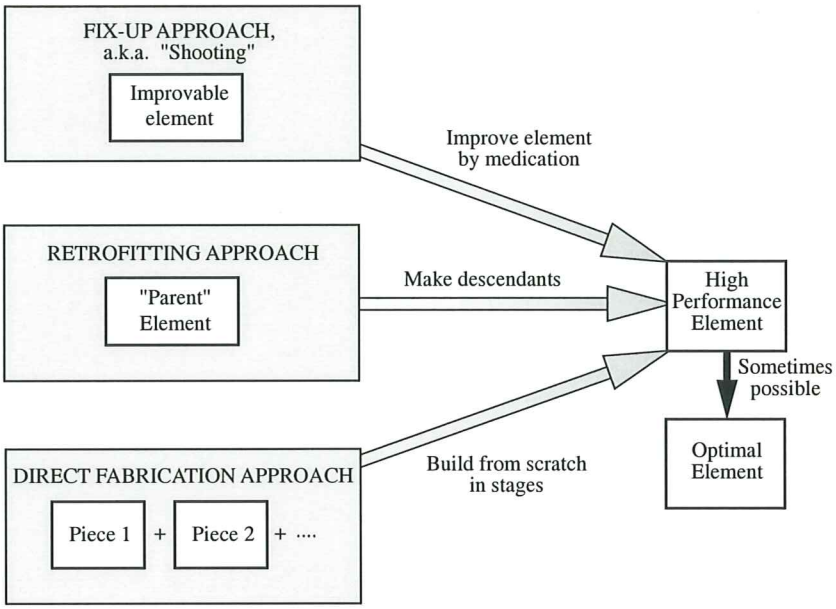

Figure 1. Element derivation approaches, not to be confused with methods.

introductory FEM course: "never, never, never use a higher order or special element unless you are absolutely sure of what you are doing" [3, Ch. 8]. The attraction of HP elements in the real world is understandable: to get reasonable answers with models that cannot stray too far from physics.

An *optimal element* is one whose performance cannot be improved for a given node-freedom configuration. The concept is fuzzy, however, unless one specifies precisely what is the optimality measure. There are often tradeoffs. For example, passing patch tests on any mesh may conflict with insensitivity to mesh distortion [2, p. 115].

One of the side effects of interest in high performance is the proliferation of elements with drilling degrees of freedom (DOFs). These are nodal rotations that are not taken as independent DOFs in conventional elements. Two well known examples are: (i) corner rotations normal to the plane of a membrane element (or to the membrane component of a shell element); (ii) three corner rotations added to solid elements. This paper considers only (i).

Why membrane drilling freedoms? Three reasons are given in the Introduction to [4]:

1. The element performance may be improved without adding midside nodes, keeping model preparation (and mesh generation) simple.
2. The extra degree of freedom is "free of charge" in programs that carry six DOFs per node, as is the case in most commercial codes.
3. It simplifies the treatment of shell intersections as well as connection of shells to beam elements.

The purpose of this paper is to review critically several approaches for the construction of these elements. To keep the exposition to a reasonable length, only triangular membrane elements with 3 corner nodes are studied.

2. ELEMENT DERIVATION APPROACHES

The term *approach* is taken here to mean a combination of methods and empirical tools to achieve a given objective. In FEM work, isoparametric, stress-assumed-hybrid and ANS (Assumed Natural Strain) formulations are methods and not approaches. An approach may zig-zag through several methods.

FEM approaches range from heuristic to highly analytical. The experience of the writer in teaching advanced FEM courses is that even bright graduate students have trouble connecting different construction methods, much as undergraduates struggle to connect mathematics and laws of nature. To help students the writer has grouped element derivation approaches into those pictured in Figure 1.

Figure 1 makes an implicit assumption: the performance of an element of given geometry, node and freedom configuration can be improved. There are obvious examples where this is not possible. For example, constant-strain elements with translational freedoms only: 2-node bar, 3-node membrane triangle and 4-node elasticity tetrahedron. Those cases are excluded because it makes no sense to talk about high performance or optimality under those conditions.

2.1. Fixing Up

Conventional element derivation methods, such as the isoparametric formulation, may produce bad or mediocre low-order elements. If that is the case two questions may be raised:

(i) Can the element be improved?

(ii) Is the improvement worth the trouble?

If the answer to both is yes, the fix-up approach tries to improve the performance by an array of remedies that may be collectively called the FEM pharmacy. Cures range from heuristic tricks such as reduced and selective integration to more scientifically based concoctions.

This approach accounts for most of the current publications in finitelementology. Playing doctor can be fun. But also frustating, as trying to find a black cat in a dark cellar at midnight. Inject these incompatible modes: oops! the patch test is violated. Make the Jacobian constant: oops! it locks in distortion. Reduce the integration order: oops! it lost rank sufficiency. Split the stress-strain equations and integrate selectively: oops! it is not observer invariant. And so on.

2.2. Retrofitting

Retrofitting is a more sedated activity. One begins with a irreproachable parent element, free of obvious defects. Typically this is a higher order iso-P element constructed with a complete or bicomplete polynomial; for example the 6-node quadratic triangle or the 9-node Lagrange quadrilateral. The parent is fine but too complicated to be an HP element. Complexity is reduced by master-slave constraint techniques so as to fit the desired node-freedom configuration pattern.

This approach commonly makes use of node and freedom migration techniques. For example, drilling freedoms may be defined by moving translational midpoint or thirdpoint freedoms to corner rotations by kinematic constraints. The development of "descendants" of the LST element discussed in Section 7 fits this approach. Discrete Kirchhoff constraints and degeneration (3D→2D) for plate and shell elements provide another example. Retrofitting has the advantage of being easy to understand and teach. It occasionally produces useful elements but rarely high performance ones.

2.3. Direct Fabrication

This approach relies on divide and conquer. To give an analogy: upon short training a FEM novice knows that a discrete system is decomposed into elements, which interact only through common freedoms. Going deeper, an element can be constructed as the superposition of components or pieces, with interactions limited through appropriate orthogonality conditions. (Mathematically, components are multifield subspaces.) Components are invisible to the user once the element is implemented.

Fabrication is done in stages. At the start there is nothing: the element is without form, and void. At each stage the developer injects another component (= subspace). Components may be done through different methods. The overarching principle is correct performance after each stage. (This is in agreement with the Pontryagin-Bellman concept of optimal multistage decision processes [5,6].) If at any stage the element has problems (for example: it locks) no retroactive cure is attempted as in the fix-up approach. Instead the component is trashed and another one picked. One never uses more components than strictly needed: condensation is forbidden. Components may contain free parameters, which may be used to improve performance and eventually to try for optimality. One general scheme for direct fabrication is the template approach [7].

All applications of the direct fabrication method to date have been done in two stages, separating the element response into basic and higher order. This process is further elaborated in Section 4.3.

2.4. A Warning

The classification of Figure 1 is based on approaches and not methods. A method may appear in more than one approach. For example, methods based on hybrid functionals may be used to retrofit or to fabricate, and even (more rarely) to fix up. Methods based on assumed strain or incompatible displacement fields may be used to do all three. This interweaving of methods and approaches is what makes so difficult to teach advanced FEM. While it is relatively easy to teach methods, choosing and pursuing an approach is a synthesis activity that relies on judgement, experience and luck.

3. A GALLERY OF TRIANGLES

This article looks at triangular membrane elements in several flavors organized along family lines. To keep track of parents and siblings it is convenient to introduce the following notational scheme for the configuration of an element:

$$\text{xST-}n/m\text{[variants][-application]} \tag{1}$$

Lead letter x is C, L or Q, which fingers the parent element as indicated below. Integers n and m give the total number of nodes and freedoms, respectively. Further distinction is made by appending letters to identify variants. For example QST-10/20C, QST-3/20G and QST-3/20RS identify the QST parent and two descendants. Here C, G and RS stand for "conventional freedoms", "gradient freedoms" and "rotational-plus-strain freedoms," respectively. The reader may see examples of this identification scheme arranged in Figure 2.

The three parent elements shown there are generated by complete polynomials. They are:

1. *Constant Strain Triangle* or CST. Also called linear triangle and Turner triangle. Developed as plane stress element by Jon Turner, Ray Clough and Harold Martin in 1952–53 [8]; published 1956 [9].

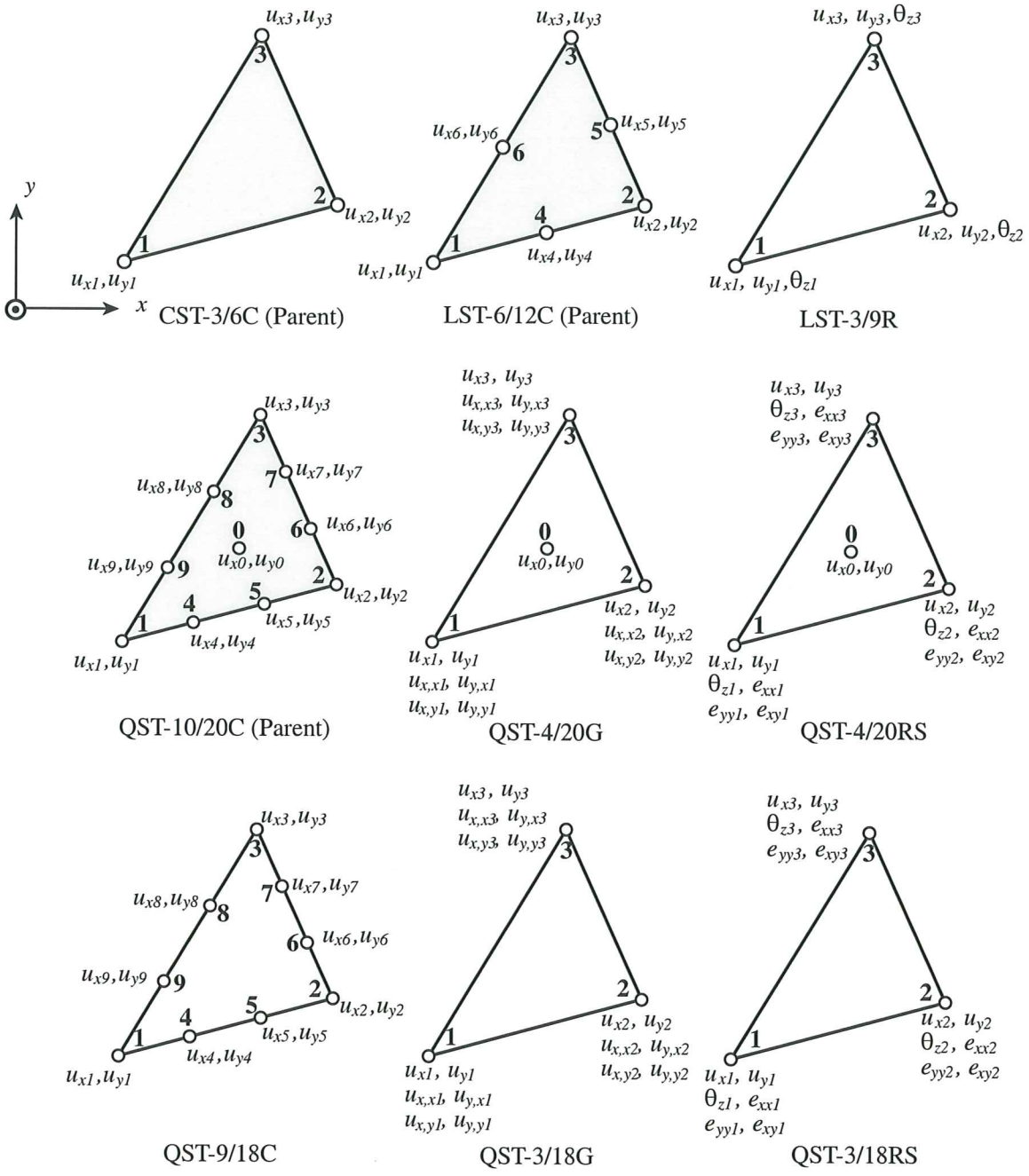

Figure 2. Node and freedom configuration of triangular membrane element families. Only non-hierarchical models with Cartesian node displacements are shown.

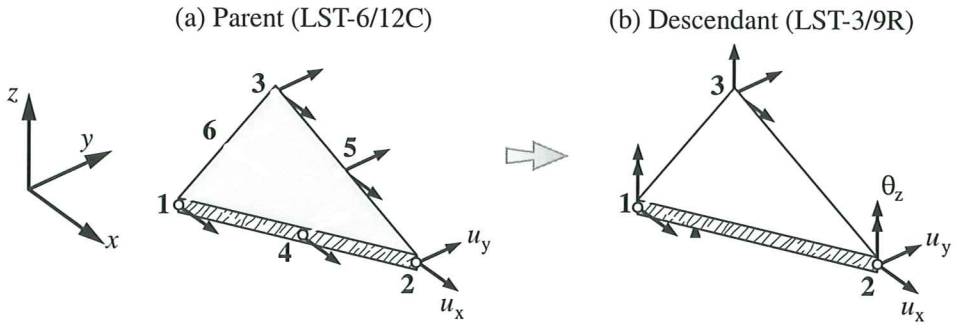

Figure 3. Node and freedom configuration of the membrane triangle LST-3/9R and its parent element LST-6/12C.

2. *Linear Strain Triangle* or LST. Also called quadratic triangle and Veubeke triangle. Developed by B. Fraeijs de Veubeke in 1962–63 [10]; published 1965 [11].

3. *Quadratic Strain Triangle* or QST. Also called cubic triangle. Developed by the writer in 1965; published 1966 [12]. Shape functions for QST-10/20RS to QST-3/18G were presented there but used for plate bending instead of plane stress; e.g., QST-3/18G clones the BCIZ element [13].

Drilling freedoms in triangles were used in static and dynamic shell analysis in Carr's thesis under Ray Clough [14,15], using QST-3/20RS as membrane component. The same idea was independently exploited for rectangular and quadrilateral elements, respectively, in the theses of Abu-Ghazaleh [16] and Willam [17], both under Alex Scordelis. A variant of the Willam quadrilateral, developed by Bo Almroth at Lockheed, has survived in the nonlinear shell analysis code STAGS as element 410 [18].

The focus of this article is on LST-3/9R, shown in the upper right corner of Figure 2 and, in 3D view, in Figure 3(b). The whole development pertains to the membrane (plane stress) problem. Thus no additional identifiers are used. Should the model be applied to a different problem, for example plane strain or axisymmetric analysis, an application identifier would be necessary under scheme (1).

4. THE ANDES TRIANGLE WITH DRILLING FREEDOMS

As pictured in in Figure 3(b), the LST-3/9R membrane triangle has 3 corner nodes and 3 DOFs per node: two inplane translations and a drilling rotation. In the retrofitting approach studied in Section 7 the parent element is the conventional Linear Strain Triangle, which is technically identified as LST-6/12C.

The direct fabrication approach was used in a three-part 1992 paper [4,19,20] to construct an optimal version of LST-3/9R. (This work grew out of student term projects in an advanced finite element course.) Two different techniques were used in that development:

EFF. The Extended Free Formulation, which is a variant of the Free Formulation (FF) of Bergan [21–29].

ANDES. The Assumed Natural DEviatoric Strain formulation, which combines the FF of Bergan and the Assumed Natural Strain (ANS) method of Park and Stanley [30,31]. ANDES has also been used to develop plate bending and shell elements [32,33].

For the LST-3/9R, these techniques led to stiffness matrices with free parameters: 3 and 7 in the

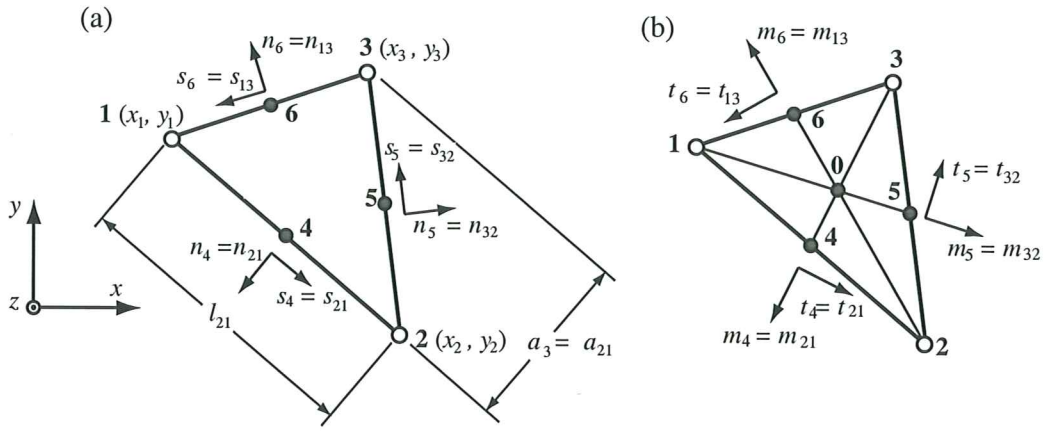

Figure 4. Triangle geometry.

case of EFF and ANDES, respectively. Free parameters were optimized so that rectangular mesh units are exact in pure bending for arbitrary aspect ratios, a technique further discussed in Section 5. Surprisingly the same optimal element was found. In the nomenclature of templates summarized in Section 4.7 the two elements are said to be *clones*. This coalescence nurtured the feeling that the optimal form is unique. More recent studies reported in Section 5.4 verify uniqueness if certain orthogonality constraints are placed on the higher order response.

4.1. Element Description

The membrane (plane stress) triangle shown in Figure 4 has straight sides joining the corners, which are defined by the coordinates $\{p_i, y_i\}$, $i = 1, 2, 3$. Coordinate differences are abbreviated $x_{ij} = x_i - x_j$ and $y_{ij} = y_i - y_j$. The signed area A is given by

$$2A = (x_2y_3 - x_3y_2) + (x_3y_1 - x_1y_3) + (x_1y_2 - x_2y_1) = y_{21}x_{13} - x_{21}y_{13} \quad \text{(and 2 others)}. \quad (2)$$

In addition to the corner nodes 1, 2 and 3 we shall also use midpoints 4, 5 and 6 for derivations although these nodes do not appear in the final equations of the LST-3/9R. Midpoints 4, 5, 6 are located opposite corners 3, 1 and 2, respectively. The centroid is denoted by 0. As shown in Figure 4, two intrinsic coordinate systems are used over each side:

$$n_{21}, s_{21}, \quad n_{32}, s_{32}, \quad n_{13}, s_{13}, \quad (3)$$

$$m_{21}, t_{21}, \quad m_{32}, t_{32}, \quad m_{13}, t_{13}. \quad (4)$$

Here n and s are oriented along the external normal-to-side and side directions, respectively, whereas m and t are oriented along the triangle median and normal-to-median directions, respectively. The coordinate sets (3)–(4) align only for equilateral triangles. The origin of these systems is left "floating" and may be adjusted as appropriate. If the origin is placed at the midpoints, subscripts 4, 5 and 6 may be used instead of 21, 32 and 13, respectively, as illustrated in Figure 4.

Other intrinsic dimensions of use in various derivations are

$$\ell_{ij} = \ell_{ji} = \sqrt{x_{ij}^2 + y_{ij}^2}, \quad a_{ij} = a_k = 2A/\ell_{ij}, \quad m_k = \tfrac{3}{2}\sqrt{x_{k0}^2 + y_{k0}^2}, \quad b_k = 2A/m_k, \quad (5)$$

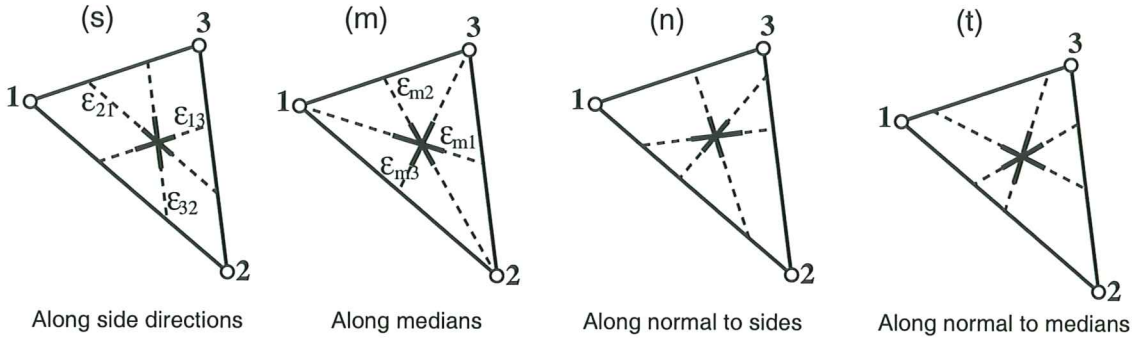

Figure 5. Four choices for natural strains. Labels (s) through (t) correlate with the notation (3)-(4). Although the "natural straingage rosettes" are pictured at the centroid for viewing convenience, they may be placed at any point on the triangle.

Here j and k denote the positive cyclic permutations of i; for example $i = 2$, $j = 3$, $k = 1$. The ℓ_{ij}'s are the lengths of the sides, $a_k = a_{ij}$ are triangle heights, m_k are the lengths of the medians, and b_k are side lengths projected on normal-to-median directions.

The well known triangle coordinates are denoted by ζ_1, ζ_2 and ζ_3, which satisfy $\zeta_1 + \zeta_2 + \zeta_3 = 1$.

The degrees of freedom of LST-3/9R are collected in the node displacement vector

$$\mathbf{u}_R = [\, u_{x1} \quad u_{y1} \quad \theta_1 \quad u_{x2} \quad u_{y2} \quad \theta_2 \quad u_{x3} \quad u_{y3} \quad \theta_3 \,]^T . \tag{6}$$

Here u_{xi} and u_{yi} denote the nodal values of the translational displacements u_x and u_y along x and y, respectively, and $\theta \equiv \theta_z$ are the "drilling rotations" about z (positive counterclockwise when looking down on the element midplane along $-z$). In continuum mechanics these rotations are defined by

$$\theta = \theta_z = \tfrac{1}{2}\left(\frac{\partial u_y}{\partial x} - \frac{\partial u_x}{\partial y}\right). \tag{7}$$

The triangle will be assumed to have constant thickness h and uniform plane stress constitutive properties defined by the 3×3 elastic modulus matrix arranged in the usual manner:

$$\mathbf{E} = \begin{bmatrix} E_{11} & E_{12} & E_{13} \\ E_{12} & E_{22} & E_{23} \\ E_{13} & E_{23} & E_{33} \end{bmatrix}. \tag{8}$$

4.2. Natural Strains

In the derivation of the higher order stiffness by ANDES [19] *natural strains* play a key role. These are extensional (direct) strains along three directions intrinsically related to the triangle geometry. Four possible choices are depicted in Figure 5. Choice (s): strains along the 3 side directions, was the one used in [19] because it matches the direction of neutral axes of the assumed inplane bending modes as discussed in Section 4.6.

The (s) natural strains are collected in the 3-vector

$$\epsilon = [\, \epsilon_{21} \quad \epsilon_{32} \quad \epsilon_{13} \,]^T . \tag{9}$$

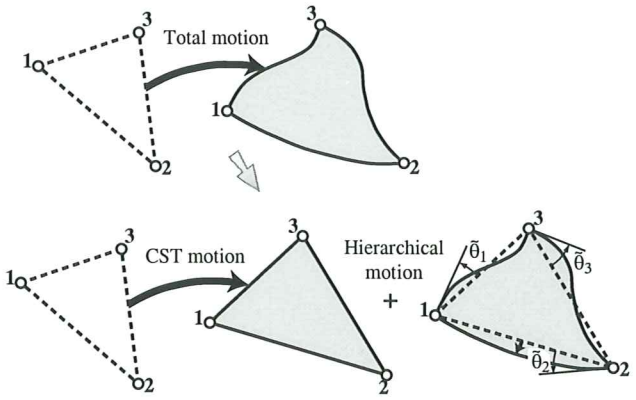

Figure 6. Decomposition of inplane motion into CST (linear displacement) + hierarchical. The same idea (in 2D or 3D) is also important in corotational formulations.

Vector ϵ at point i is denoted by ϵ_i. The natural strain ϵ_{jk} at point i will be written $\epsilon_{jk|i}$, the bar being used for reading convenience. The natural strains are related to Cartesian strains $\{e_{xx}, e_{yy}, 2e_{xy}\}$ by the "straingage rosette" transformation

$$\boldsymbol{\epsilon} = \begin{bmatrix} \epsilon_{12} \\ \epsilon_{23} \\ \epsilon_{31} \end{bmatrix} = \begin{bmatrix} x_{21}^2/\ell_{21}^2 & y_{21}^2/\ell_{21}^2 & x_{21}y_{21}/\ell_{21}^2 \\ x_{32}^2/\ell_{32}^2 & y_{32}^2/\ell_{32}^2 & x_{32}y_{32}/\ell_{32}^2 \\ x_{13}^2/\ell_{13}^2 & y_{13}^2/\ell_{13}^2 & x_{13}y_{13}/\ell_{13}^2 \end{bmatrix} \begin{bmatrix} e_{xx} \\ e_{yy} \\ 2e_{xy} \end{bmatrix} = \mathbf{T}_e^{-1}\mathbf{e}, \tag{10}$$

in which $\ell_{ji}^2 = x_{ji}^2 + y_{ji}^2$. The inverse relation is

$$\begin{bmatrix} e_{xx} \\ e_{yy} \\ 2e_{xy} \end{bmatrix} = \frac{1}{4A^2} \begin{bmatrix} y_{23}y_{13}\ell_{21}^2 & y_{31}y_{21}\ell_{32}^2 & y_{12}y_{32}\ell_{13}^2 \\ x_{23}x_{13}\ell_{21}^2 & x_{31}x_{21}\ell_{32}^2 & x_{12}x_{32}\ell_{13}^2 \\ (y_{23}x_{31}+x_{32}y_{13})\ell_{21}^2 & (y_{31}x_{12}+x_{13}y_{21})\ell_{32}^2 & (y_{12}x_{23}+x_{21}y_{32})\ell_{13}^2 \end{bmatrix} \begin{bmatrix} \epsilon_{12} \\ \epsilon_{23} \\ \epsilon_{31} \end{bmatrix}, \tag{11}$$

or, in compact matrix notation, $\mathbf{e} = \mathbf{T}_e\boldsymbol{\epsilon}$. Note that $\mathbf{T}_e$ is constant over the triangle. The natural stress-strain matrix $\mathbf{E}_{nat}$ is defined by

$$\mathbf{E}_{nat} = \mathbf{T}_e^T\mathbf{E}\mathbf{T}_e, \tag{12}$$

which is also constant over the triangle.

4.3. Hierarchical Rotations

Hierarchical drilling freedoms are useful for compactly expressing the higher order behavior of the element. Their geometric interpretation is shown in Figure 6. To extract the hierarchical corner rotations $\tilde{\theta}_i$ from the total corner rotations θ_i, subtract the mean or CST rotation θ_0:

$$\tilde{\theta}_i = \theta_i - \theta_0, \tag{13}$$

where $i = 1, 2, 3$ is the corner index and

$$\theta_0 = \frac{1}{4A}\left(x_{23}u_{x1} + x_{31}u_{x2} + x_{12}u_{x3} + y_{23}u_{y1} + y_{31}u_{y2} + y_{12}u_{y3}\right). \tag{14}$$

Applying (13)-(14) to the three corners we assemble the transformation

$$\tilde{\boldsymbol{\theta}} = \begin{bmatrix} \tilde{\theta}_1 \\ \tilde{\theta}_2 \\ \tilde{\theta}_3 \end{bmatrix} = \frac{1}{4A} \begin{bmatrix} x_{32} & y_{32} & 4A & x_{13} & y_{13} & 0 & x_{21} & y_{21} & 0 \\ x_{32} & y_{32} & 0 & x_{13} & y_{13} & 4A & x_{21} & y_{21} & 0 \\ x_{32} & y_{32} & 0 & x_{13} & y_{13} & 0 & x_{21} & y_{21} & 4A \end{bmatrix} \begin{bmatrix} u_{x1} \\ u_{y1} \\ \theta_1 \\ u_{x2} \\ u_{y2} \\ \theta_2 \\ u_{x3} \\ u_{y3} \\ \theta_3 \end{bmatrix} = \tilde{\mathbf{T}}_{\theta u} \mathbf{u}_R. \quad (15)$$

For some developments it is useful to complete this transformation with the identity matrix for the translational freedoms:

$$\tilde{\mathbf{u}}_R = \begin{bmatrix} u_{x1} \\ u_{y1} \\ \tilde{\theta}_1 \\ u_{x2} \\ u_{y2} \\ \tilde{\theta}_2 \\ u_{x3} \\ u_{y3} \\ \tilde{\theta}_3 \end{bmatrix} = \begin{bmatrix} 1 & 0 & 0 & 0 & 0 & 0 & 0 & 0 & 0 \\ 0 & 1 & 0 & 0 & 0 & 0 & 0 & 0 & 0 \\ \frac{x_{32}}{4A} & \frac{y_{32}}{4A} & 1 & \frac{x_{13}}{4A} & \frac{y_{13}}{4A} & 0 & \frac{x_{21}}{4A} & \frac{y_{21}}{4A} & 0 \\ 0 & 0 & 0 & 1 & 0 & 0 & 0 & 0 & 0 \\ 0 & 0 & 0 & 0 & 1 & 0 & 0 & 0 & 0 \\ \frac{x_{32}}{4A} & \frac{y_{32}}{4A} & 0 & \frac{x_{13}}{4A} & \frac{y_{13}}{4A} & 1 & \frac{x_{21}}{4A} & \frac{y_{21}}{4A} & 0 \\ 0 & 0 & 0 & 0 & 0 & 0 & 1 & 0 & 0 \\ 0 & 0 & 0 & 0 & 0 & 0 & 0 & 1 & 0 \\ \frac{x_{32}}{4A} & \frac{y_{32}}{4A} & 0 & \frac{x_{13}}{4A} & \frac{y_{13}}{4A} & 0 & \frac{x_{21}}{4A} & \frac{y_{21}}{4A} & 1 \end{bmatrix} \begin{bmatrix} u_{x1} \\ u_{y1} \\ \theta_1 \\ u_{x2} \\ u_{y2} \\ \theta_2 \\ u_{x3} \\ u_{y3} \\ \theta_3 \end{bmatrix} = \tilde{\mathbf{T}}_R \mathbf{u}_R. \quad (16)$$

The inverse transformation $\tilde{\mathbf{T}}_R^{-1}$ that connects $\mathbf{u}_R = \tilde{\mathbf{T}}_R^{-1} \tilde{\mathbf{u}}_R$ is obtained by simply transposing the subscripts in the coordinate differences; $x_{32} \to -x_{32} = x_{23}$, etc. The foregoing transformation matrices are constant over the element.

4.4. The Stiffness Template

The fundamental element stiffness decomposition of the two-stage direct fabrication method is

$$\mathbf{K} = \mathbf{K}_b + \mathbf{K}_h \quad (17)$$

Here $\mathbf{K}_b$ is the basic stiffness, which takes care of consistency, and $\mathbf{K}_h$ is the higher order stiffness, which takes care of stability (rank sufficiency) and accuracy. This decomposition was found by Bergan and Nygård [22] as part of the Free Formulation (FF) but actually holds for any element that passes the Individual Element Test (IET) of Bergan and Hanssen [34]. (The IET is a strong form of the patch test that demands pairwise cancellation of tractions between adjacent elements in constant stress states.) Similar elements were constructed by Belytschko and coworkers [35] using an hourglass stabilization approach. See also Hughes [36, §4.8].

Orthogonality conditions satisfied by $\mathbf{K}_h$ are discussed in [21,23–29,37–41].

The EFF and ANDES triangles derived in [4] and [19] initially carry along a set of free numerical parameters, most of which affect the higher order stiffness:

$$\mathbf{K}^{\text{EFF'91}}(\alpha_b, \alpha_h, \gamma) = \mathbf{K}_b(\alpha_b) + (1-\gamma)\mathbf{K}_h^u(\alpha_h), \quad (18)$$

$$\mathbf{K}^{\text{ANDES'91}}(\alpha_b, \beta, \rho_1, \ldots \rho_5) = \mathbf{K}_b(\alpha_b) + \beta \mathbf{K}_h^u(\rho_1, \ldots \rho_5), \tag{19}$$

where $\mathbf{K}_h^u$ is the unscaled higher order stiffness. Both $\mathbf{K}_b$ and $\mathbf{K}_h$ must have rank 3. Algebraic forms such as (18)-(19) possessing free parameters are called *element stiffness templates* or simply *templates*.

The basic stiffness $\mathbf{K}_b(\alpha_b)$ is identical for both (18) and (19). In fact, patch test and template theory [7,37–41] says that $\mathbf{K}_b(\alpha_b)$ must be shared by all elements that pass the IET although α_b may vary. However α_b must be the same for all LST-3/9R elements connected in an assembly, for otherwise the patch test would be violated. This is called a *mixability condition*. Parameters other than α_b may, in principle, vary from element to element without affecting convergence.

4.5. The Basic Stiffness

The explicit form of the basic stiffness for the LST-3/9R configuration was obtained in 1984 and published the following year [23]. It can be expressed as

$$\mathbf{K}_b = V^{-1}\mathbf{L}\,\mathbf{E}\,\mathbf{L}^T. \tag{20}$$

where $V = Ah$ is the element volume, and $\mathbf{L}$ is a 3×9 matrix that contains a free parameter α_b:

$$\mathbf{L} = \tfrac{1}{2}h \begin{bmatrix} y_{23} & 0 & x_{32} \\ 0 & x_{32} & y_{23} \\ \frac{1}{6}\alpha_b y_{23}(y_{13}-y_{21}) & \frac{1}{6}\alpha_b x_{32}(x_{31}-x_{12}) & \frac{1}{3}\alpha_b(x_{31}y_{13}-x_{12}y_{21}) \\ y_{31} & 0 & x_{13} \\ 0 & x_{13} & y_{31} \\ \frac{1}{6}\alpha_b y_{31}(y_{21}-y_{32}) & \frac{1}{6}\alpha_b x_{13}(x_{12}-x_{23}) & \frac{1}{3}\alpha_b(x_{12}y_{21}-x_{23}y_{32}) \\ y_{12} & 0 & x_{21} \\ 0 & x_{21} & y_{12} \\ \frac{1}{6}\alpha_b y_{12}(y_{32}-y_{13}) & \frac{1}{6}\alpha_b x_{21}(x_{23}-x_{31}) & \frac{1}{3}\alpha_b(x_{23}y_{32}-x_{31}y_{13}) \end{bmatrix}. \tag{21}$$

In the FF this is called a *force-lumping matrix*, hence the symbol $\mathbf{L}$. Under conditions discussed in [29,39] $\mathbf{L}$ can be related to the mean strain-displacement matrix $\mathbf{B}_0$ or $\bar{\mathbf{B}}$ used in one-point reduced integration schemes: $\mathbf{B}_0 = \mathbf{L}^T/V$, for specific choices of α_b. This matrix also appears in the so-called "B-bar" formulation [36]. If $\alpha_b = 0$ the basic stiffness reduces to the total stiffness matrix of the CST-3/6C, in which case the rows and columns associated with the drilling rotations vanish.

One interesting result is that

$$\mathbf{L}^T = \mathbf{L}^T\tilde{\mathbf{T}}_R, \quad (\text{also } \mathbf{B}_0 = \mathbf{B}_0\tilde{\mathbf{T}}_R\,), \tag{22}$$

for any α_b, which shows that the transformation (16) projects out the higher order behavior.

The deep significance of this development is: *the basic stiffness of any element with this node-freedom configuration that passes the IET must have the form* (20)–(21). Most derivation methods produce the total stiffness $\mathbf{K}$ directly, with $\mathbf{K}_b$ concealed behind the scenes. This is one of the reasons accounting for the capricious nature of the fix-up approach. In the direct fabrication approach the decomposition (17) is explicitly used in the two-stage construction of the element: first $\mathbf{K}_b$ and then $\mathbf{K}_h$.

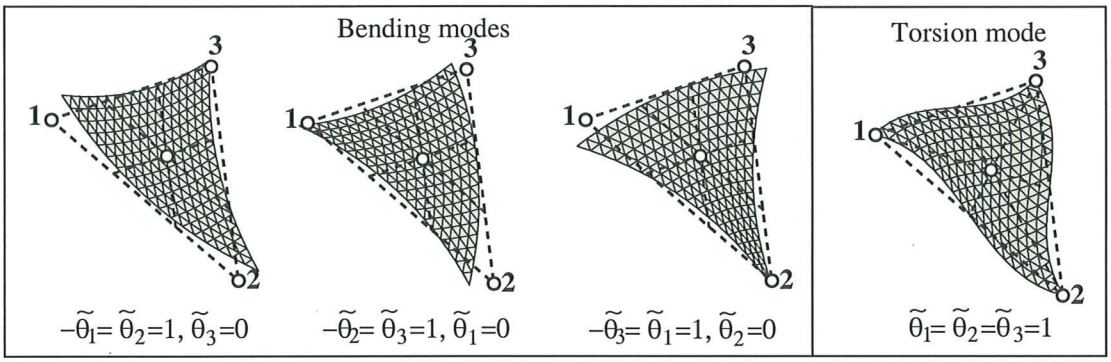

Figure 7. Patterns chosen to build the higher order stiffness of the ANDES template (31): three bending-along-sides modes plus a torsion mode. Although pictured as displacement motions for visualization convenience, the bending modes were initially assumed in natural strains as described in Appendix A. The "neutral axes" of the bending modes are parallel to the sides and pass through the centroid.

4.6. The Higher Order Stiffness

We describe here essentially the ANDES form of $\mathbf{K}_h$ developed in [19], with some generalizations in the set of free parameters. The higher order stiffness matrix is

$$\mathbf{K}_h = c_{fac}\tilde{\mathbf{T}}_{\theta u}^T \mathbf{K}_\theta \tilde{\mathbf{T}}_{\theta u}. \tag{23}$$

where $\mathbf{K}_\theta$ is the 3×3 higher order stiffness in terms of the hierarchical rotations $\tilde{\boldsymbol{\theta}}$ of (13), $\mathbf{T}_{\tilde{\theta}u}$ is the matrix (15), and c_{fac} is a scaling factor to be determined later. To construct $\mathbf{K}_\theta$ by ANDES one picks deviatoric natural strain patterns, in which "deviatoric" means change from the constant strain states.

Since the main objective is to have good inplane bending behavior, it is logical to begin by assuming patterns associated with three bending-like modes. A key question is, along which directions? For a triangle, four choices — already depicted in Figure 5 as regards the definition of natural strains — satisfy observer invariance:

Along the side directions s_4, s_5, s_6 (23)

Along the normal directions n_4, n_5, n_6 (24)

Along the median directions m_4, m_5, m_6 (25)

Along the normal-to-the-median directions t_4, t_5, t_6 (26)

Choice (23) was adopted in [19]. The three bending strain patterns are sketched on the left of Figure 7 as displacement modes for visualization convenience. (The bending shapes pictured there were obtained by integrating the assumed strain fields and adjusting rigid body motions.) It turns out that the three patterns are not linearly independent: their sum vanishes for any triangle geometry. Thus use of only those modes would produce a rank deficient $\mathbf{K}_h$.

To attain the correct rank of 3 the "torsion" pattern depicted on the right of Figure 7 is adjoined. This can be visualized as produced by applying identical hierarchical rotations $\tilde{\theta}_1 = \tilde{\theta}_2 = \tilde{\theta}_3$. A

cubic displacement pattern was constructed from the QST-4/20G interpolation. The associated quadratic strain pattern was transformed to natural strains and filtered to a linear one by midpoint collocation. These derivations are presented in Appendix A for readers interested in the details.

To express $\mathbf{K}_\theta$ compactly, introduce the following matrices, which depend on nine free dimensionless parameters, β_1 through β_9:

$$\mathbf{Q}_1 = \frac{2A}{3}\begin{bmatrix} \frac{\beta_1}{\ell_{21}^2} & \frac{\beta_2}{\ell_{21}^2} & \frac{\beta_3}{\ell_{21}^2} \\ \frac{\beta_4}{\ell_{32}^2} & \frac{\beta_5}{\ell_{32}^2} & \frac{\beta_6}{\ell_{32}^2} \\ \frac{\beta_7}{\ell_{13}^2} & \frac{\beta_8}{\ell_{13}^2} & \frac{\beta_9}{\ell_{13}^2} \end{bmatrix}, \quad \mathbf{Q}_2 = \frac{2A}{3}\begin{bmatrix} \frac{\beta_9}{\ell_{21}^2} & \frac{\beta_7}{\ell_{21}^2} & \frac{\beta_8}{\ell_{21}^2} \\ \frac{\beta_3}{\ell_{32}^2} & \frac{\beta_1}{\ell_{32}^2} & \frac{\beta_2}{\ell_{32}^2} \\ \frac{\beta_6}{\ell_{13}^2} & \frac{\beta_4}{\ell_{13}^2} & \frac{\beta_5}{\ell_{13}^2} \end{bmatrix}, \quad \mathbf{Q}_3 = \frac{2A}{3}\begin{bmatrix} \frac{\beta_5}{\ell_{21}^2} & \frac{\beta_6}{\ell_{21}^2} & \frac{\beta_4}{\ell_{21}^2} \\ \frac{\beta_8}{\ell_{32}^2} & \frac{\beta_9}{\ell_{32}^2} & \frac{\beta_7}{\ell_{32}^2} \\ \frac{\beta_3}{\ell_{13}^2} & \frac{\beta_1}{\ell_{13}^2} & \frac{\beta_2}{\ell_{13}^2} \end{bmatrix}. \tag{28}$$

The scaling by $2A/3$ is for convenience in correlating with prior developments. Matrix $\mathbf{Q}_i$ relates the natural strains ϵ_i at corner i to the deviatoric corner curvatures $\tilde{\theta}$. At a point of triangular coordinates $\{\zeta_1, \zeta_2, \zeta_3\}$, $\epsilon = \mathbf{Q}\,\tilde{\theta}$ where $\mathbf{Q} = \mathbf{Q}_1\zeta_1 + \mathbf{Q}_2\zeta_2 + \mathbf{Q}_3\zeta_3$. Evaluate this at the midpoints:

$$\mathbf{Q}_4 = \tfrac{1}{2}(\mathbf{Q}_1 + \mathbf{Q}_2), \quad \mathbf{Q}_5 = \tfrac{1}{2}(\mathbf{Q}_2 + \mathbf{Q}_3), \quad \mathbf{Q}_6 = \tfrac{1}{2}(\mathbf{Q}_3 + \mathbf{Q}_1) \tag{29}$$

Then

$$\mathbf{K}_\theta = h\left(\mathbf{Q}_4^T\mathbf{E}_{nat}\mathbf{Q}_4 + \mathbf{Q}_5^T\mathbf{E}_{nat}\mathbf{Q}_5 + \mathbf{Q}_6^T\mathbf{E}_{nat}\mathbf{Q}_6\right), \tag{30}$$

and $\mathbf{K}_h = \frac{3}{4}\beta_0\mathbf{T}_{\theta u}^T\mathbf{K}_\theta\mathbf{T}_{\theta u}$, where β_0 is an overall scaling coefficient. (This coefficient could be absorbed into the β_i but it is left separate to simplify the incorporation of material behavior into the optimal element.) So finally $\mathbf{K}_R$ assumes a template form with 11 free parameters: $\alpha_b, \beta_0, \beta_1, \ldots \beta_9$:

$$\mathbf{K}_R(\alpha_b, \beta_0, \beta_1, \ldots \beta_9) = V^{-1}\mathbf{L}\mathbf{E}\mathbf{L}^T + \tfrac{3}{4}\beta\,\tilde{\mathbf{T}}_{\theta u}^T\,\mathbf{K}_\theta\,\tilde{\mathbf{T}}_{\theta u}. \tag{31}$$

The factor $\frac{3}{4}$ in $\mathbf{K}_h$ comes from "historical grandfathering": as shown in Section 5 the optimal β_0 for $\nu = 0$ becomes $\frac{1}{2}$, same as in the 1984 Free Formulation element [23].

The template (31) will be called the "LST-3/9R ANDES Template" to distinguish it from others alluded to in Section 4.9.

It is easily checked that if the 3×3 matrix with $\{\beta_1, \beta_2, \beta_3\}$, $\{\beta_4, \beta_5, \beta_6\}$ and $\{\beta_7, \beta_8, \beta_9\}$ as rows is nonsingular, then $\mathbf{Q}_1$, $\mathbf{Q}_2$ and $\mathbf{Q}_3$ have full rank for $A \neq 0$ and nonzero side lengths. With the usual restrictions on the stress-strain matrix $\mathbf{E}$, $\mathbf{K}_\theta$ then has full rank of 3 and $\mathbf{K}_R$ is rank sufficient.

The parameter set in (28) is more general than that used in [19]. That development had only five free parameters in the $\mathbf{Q}_i$ matrices: ρ_1 through ρ_5, cf. (19), which enforced *a priori* the triangular symmetry conditions

$$\beta_7 = -\beta_1, \quad \beta_8 = -\beta_3, \quad \beta_9 = -\beta_2. \tag{32}$$

These constraints may be derived, for example, by taking an equilateral triangle in which $\ell_{21} = \ell_{32} = \ell_{13}$ and looking at symmetries about the medians as the $\tilde{\theta}_i$ are applied to each corner in turn. Furthermore the torsional mode was not parametrized in [19]. The present parameter set is able to encompass elements, such as the retrofitted LST, where that mode is missing.

Table 1. Identifier of Triangle Element Instances

Name	Description	See
ALL-3I	Allman 88 element integrated by 3-point interior rule.	Section 8
ALL-3M	Allman 88 element integrated by 3-midpoint rule.	Section 8
ALL-EX	Allman 88 element, exactly integrated	Section 8
ALL-LS	Allman 88 element, least-square strain fit.	Section 8
CST	Constant strain triangle CST-3/6C.	Ref. [9]
FF84	1984 Free Formulation element of Bergan and Felippa.	Ref. [23]
LST-Ret	Retrofitted LST with $\alpha_b = 4/3$.	Section 7
OPT	Optimal ANDES Template.	Section 5.2

Table 2. Signatures of Some LST-3/9R Instances Befitting the ANDES Template (31)

Name	α_b	β_0	β_1	β_2	β_3	β_4	β_5	β_6	β_7	β_8	β_9
ALL-3I	1	4/9	1/12	5/12	1/2	0	1/3	−1/3	−1/12	−1/2	−5/12
ALL-3M	1	4/9	1/4	5/4	3/2	0	1	−1	−1/4	−3/2	−5/4
ALL-EX	not an instance of ANDES template										
ALL-LS	1	4/9	3/20	3/4	9/10	0	3/5	−3/5	−3/20	−9/10	−3/4
CST	0	any	0	0	0	0	0	0	0	0	0
FF84	not an instance of ANDES template										
LST-Ret	4/3	1/2	2/3	−2/3	0	0	−4/3	4/3	−2/3	0	2/3
OPT	3/2	$\frac{1}{2}(1-4\nu^2)$	1	2	1	0	1	−1	−1	−1	−2

4.7. Instances, Signatures, Clones

An element generated by specifying numerical values to the parameters $\{\alpha_b, \beta_0, \beta_1, \ldots \beta_9\}$ is a *template instance*. The set of parameter values is the *template signature*. Two elements with the same signature, possibly derived through different methods, are called *clones*.

Table 1 lists triangular elements compared later in this paper. Table 2 defines their signatures if they happen to be instances of the ANDES template (31).

By construction all template instances verify exactly the IET for rigid body modes and uniform strain/stress states. Here we see the key advantage of the direct fabrication approach: any template instance that keeps the correct rank is guaranteed to be consistent and stable. Since surprises are mitigated the task of optimizing the element, covered in Section 5, is straightforward.

4.8. Energy Orthogonality

For future use the following definition is noted. An element with linearly varying higher order strains is called *energy orthogonal* in the sense of Bergan [21] if $\mathbf{Q} = \mathbf{Q}_1\zeta_1 + \mathbf{Q}_2\zeta_2 + \mathbf{Q}_3\zeta_3$ vanishes

at the centroid $\zeta_1 = \zeta_2 = \zeta_3 = 1/3$. This gives the algebraic condition

$$\mathbf{Q}_1 + \mathbf{Q}_2 + \mathbf{Q}_3 = \mathbf{0}. \tag{33}$$

For the matrices (28), condition (33) translates to $\beta_1+\beta_5+\beta_9 = \beta_2+\beta_6+\beta_7 = \beta_3+\beta_4+\beta_8 = 0$. These conditions will not be enforced *a priori*. The optimal element derived in Section 5, however, is found to satisfy energy orthogonality.

For more general strain variations energy orthogonality conditions are discussed in [21,23–29,37–41].

4.9. Other Templates

Three more templates for $\mathbf{K}_h$ may be generated by choosing bending patterns according to the prescriptions (23), (24) or (25) for the bending modes. This has not been done to date and remains an open research problem. The closest attempt in this direction was the development of the 1984 FF element described in [23,24] by assuming bending modes along the 3 median directions. Because the FF was used, the modes were initially constructed in displacement form. An advantage of this choice is that the three modes are linearly independent and there is no need to adjoin the torsional mode. But perfect optimality in the sense discussed below was not attainable. As there are indications that the optimal element derivable from (31) is unique (cf. Section 5.4), there seems to be no compelling incentives for exploring other templates.

5. FINDING THE BEST

A template such as (31) generates an infinity of element instances by assigning numeric values to the free parameters. The obvious question is: among all those instances, is there a best one? Because all template instances pass the IET for basic modes (rigid body motions and constant strain states) any optimality criterion must necessarily rely on higher order patch tests. The obvious tests involve the response of regular mesh units to inplane bending along the side directions. This leads to element bending tests expressed as energy ratios. These have been used since 1984 to tune up the higher order stiffness of triangular elements [23,26].

5.1. The Bending Test

The x-bending test is defined in Figure 8. A Bernoulli-Euler plane beam of thin rectangular cross-section with span L, height b and thickness h (normal to the plane of the figure) is bent under applied end moments M_x. The beam is fabricated of isotropic material with elastic modulus E and Poisson's ratio ν. Except for possible end effects the exact solution of the beam problem (from both the theory-of-elasticity and beam-theory standpoints) is a constant bending moment $M(x) = M_x$ along the span. The stress field is $\sigma_{xx} = M_x\, y/I_{zz}$, $\sigma_{yy} = \sigma_{xy} = 0$, where $I_{zz} = \frac{1}{12}hb^3$. Computing the strain field $\mathbf{e} = \mathbf{E}^{-1}\boldsymbol{\sigma}$ and integrating it one finds the associated displacement field

$$u_x = -\kappa xy, \quad u_y = \tfrac{1}{2}\kappa(x^2 + \nu y^2), \tag{34}$$

where κ is the deformed beam curvature M_x/EI_{zz}. The internal energy taken up by a Bernoulli-Euler beam segment of length a is $U_x^{\text{beam}} = M_x\kappa a = 6aEM_x^2/(b^3h)$.

To test the ANDES template, the beam is modeled with one layer of identical rectangular mesh units dimensioned $a \times b$ and made up of two LST-3/9R triangles, as illustrated in Figure 9. The aspect

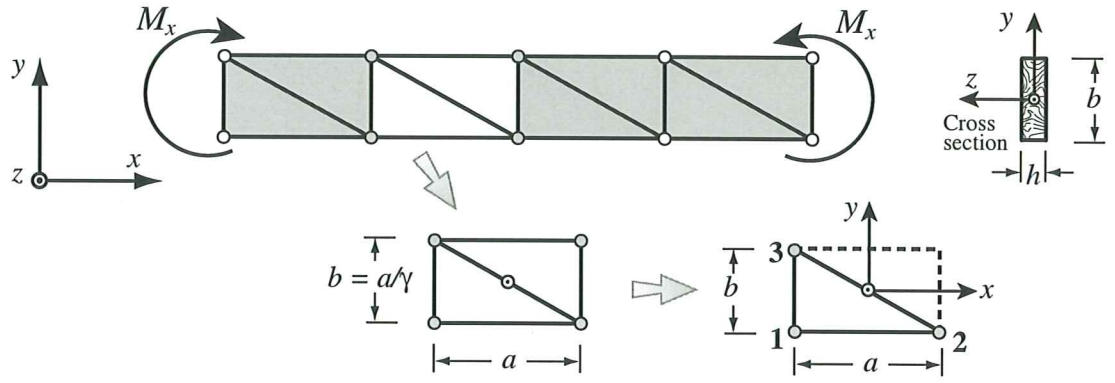

Figure 8. Constant-moment inplane bending test along the x direction.

ratio a/b is called γ. All rectangles will undergo the same deformations and stresses. We can therefore consider a typical mesh unit. Both triangles will absorb the same energy so it is sufficient to take one triangle and multiply by two. For simplicity begin by taking $\nu = 0$. Evaluating (34) at nodes 1-2-3 of the triangle shown at the bottom right of Figure 8 we get the node displacement vector

$$\mathbf{u}_x^{\text{trig}} = \frac{3M_x E\gamma^2}{a^2 h}\,[\,-a \quad \tfrac{1}{2}\gamma a \quad -2\gamma \quad a \quad \tfrac{1}{2}\gamma a \quad 2\gamma \quad a \quad \tfrac{1}{2}\gamma a \quad -2\gamma\,]^T \tag{35}$$

The strain energy absorbed by the triangle under these applied node displacements is $U_x^{\text{trig}} = \frac{1}{2}(\mathbf{u}_x^{\text{trig}})^T\mathbf{K}\mathbf{u}_x^{\text{trig}}$. That absorbed by the two-triangle mesh unit is $U_x^{quad} = 2U_x^{\text{trig}}$. The bending energy ratio computed by *Mathematica* can be expressed as

$$r = \frac{U_x^{\text{quad}}}{U_x^{\text{beam}}} = c_0 + c_2\,\gamma^2 + c_4\,\gamma^4, \tag{36}$$

where c_0, c_2 and c_4 are only functions of the free parameters. For the ensuing derivation we use the parameters of (31), but under the symmetry constraints (32) that effectively reduce the 11 parameters to 8: $\alpha_b, \beta_0, \beta_1, \ldots \beta_6$. Introduce the 6-vector $\boldsymbol{\beta} = [\,\beta_1 \quad \beta_2 \quad \beta_3 \quad \beta_4 \quad \beta_5 \quad \beta_6\,]$. Then a compact form of the coefficients is

$$c_0 = \frac{1}{3}(\alpha_b - 6)\alpha_b + \frac{\beta_0}{64}(\boldsymbol{\beta}^T\mathbf{C}_0\boldsymbol{\beta}), \quad c_2 = \frac{2}{3}(\alpha_b - 3)\alpha_b + \frac{\beta_0}{64}(\boldsymbol{\beta}^T\mathbf{C}_2\boldsymbol{\beta}), \quad c_4 = \frac{\beta_0}{64}(\boldsymbol{\beta}^T\mathbf{C}_4\boldsymbol{\beta}), \tag{37}$$

in which $\mathbf{C}$ are the symmetric matrices

$$\mathbf{C}_0 = \begin{bmatrix} 13 & -11 & -1 & 2 & 2 & -6 \\ -11 & 13 & -1 & -2 & -2 & 6 \\ -1 & -1 & 1 & 0 & 0 & 0 \\ 2 & -2 & 0 & 1 & 1 & -3 \\ 2 & -2 & 0 & 1 & 1 & -3 \\ -6 & 6 & 0 & -3 & -3 & 9 \end{bmatrix}, \mathbf{C}_2 = \begin{bmatrix} 26 & -20 & -4 & -10 & 12 & -6 \\ -20 & 22 & -2 & 8 & -14 & 8 \\ -4 & -2 & 6 & 0 & 2 & 0 \\ -10 & 8 & 0 & 5 & -5 & 1 \\ 12 & -14 & 2 & -5 & 9 & -5 \\ -6 & 8 & 0 & 1 & -5 & 5 \end{bmatrix}, \mathbf{C}_4 = \begin{bmatrix} 1 & 1 & -3 & 0 & 0 & 0 \\ 1 & 1 & -3 & 0 & 0 & 0 \\ -3 & -3 & 9 & 0 & 0 & 0 \\ 0 & 0 & 0 & 9 & -3 & -3 \\ 0 & 0 & 0 & -3 & 1 & 1 \\ 0 & 0 & 0 & -3 & 1 & 1 \end{bmatrix} \tag{38}$$

The energy ratio (36) happens to be the ratio of the exact (beam) displacement solution to that of the 2D solution. Hence $r = 1$ means that we get the exact answer, that is, the LST-3/9R element is

x-bending exact. If $r > 1$ or $r < 1$ the triangle is overstiff or overflexible in x bending, respectively. In particular, if $r >> 1$ as $a/b = \gamma$ grows the element is said to experience *aspect ratio locking* along the x direction.

The treatment of energy balance in y bending for rectangular mesh units stacked in the y direction only entails replacing γ by $1/\gamma$. Therefore if the element is x-bending optimal in the sense discussed below it is also y-bending optimal and the analysis need not be repeated.

5.2. Optimality

If $r = 1$ for any aspect ratio γ the element is called *bending optimal*. From (36) optimality requires

$$c_0 = 1, \quad c_2 = 0, \quad c_4 = 0, \quad \text{for all } \gamma = a/b \text{ and real parameter values.} \tag{39}$$

The last proviso means that complex solutions for template parameters are not admissible. The solution method is explained in Appendix B. It gives the optimal parameter set

$$\alpha_b = \tfrac{3}{2},\ \beta_0 = \tfrac{1}{2},\ \beta_1 = \beta_3 = \beta_5 = 1,\ \beta_2 = 2, \beta_4 = 0,\ \beta_6 = \beta_7 = \beta_8 = -1,\ \beta_9 = -2, \tag{40}$$

and the $\mathbf{Q}_i$ matrices found in [19] are recovered. It is easily verified that $r = r_b + r_h = 3/4 + 1/4$, where r_b and r_h come from energy taken by the basic and higher-order stiffnesses, respectively. That is, for the optimal element the basic energy accounts for 75% of the exact beam energy.

The symbolic analysis for an arbitrary ν is similar and shows that only β_0 needs to be changed:

$$\alpha_b = \tfrac{3}{2},\ \beta_0 = \tfrac{1}{2}(1-4\nu^2),\ \beta_1 = \beta_3 = \beta_5 = 1,\ \beta_2 = 2,\ \beta_4 = 0,\ \beta_6 = \beta_7 = \beta_8 = -1,\ \beta_9 = -2. \tag{41}$$

In this case $r_h = \frac{1}{4}(1 - 4\nu^2)$ so for $\nu = \frac{1}{2}$ the basic stiffness takes up all the bending energy. Since for $\nu = \frac{1}{2}$ the optimal β is 0, the higher order stiffness would vanish and the element is rank deficient. To maintain stability one sets a tiny minimum β, for example $\beta = \max(\frac{1}{2}(1-4\nu^2), 0.01)$ is used in our shell codes.

For an orthotropic material with principal material axes aligned with $\{x, y\}$ use $\nu = \sqrt{\nu_{12}\nu_{21}}$ in (41). For an arbitrary anisotropic material the optimal parameter set is not known, but it is conjectured to involve only changes in β_0.

Table 3 gives bending ratios for the elements listed in Table 1, along with numerical values for $\nu = 1/4$ and $\gamma = 1, 2, 4, 16$. Those quoted for elements other than OPT are derived in Sections 7 and 8.

5.3. Multiple Element Layers

Results of the energy bending test can be readily extended to predict the behavior of $2n$ ($n = 1, 2, \ldots$) identical layers of elements symmetrically placed through the beam height. If γ stays constant, the energy ratio becomes

$$r^{(2n)} = \frac{2^{2n} - 1 + r}{2^{2n}}, \tag{42}$$

where r is the ratio (36) for one layer, as in the configuration of Figure 8. If $r \equiv 1$, $r^{2n} \equiv 1$ so bending exactness is maintained, as can be expected. For example, if $n = 1$ (two element layers), $r^{(2)} = (3 + r)/4$. This is actually the ratio reported in Reference [20].

Table 3 Bending Energy Ratios r for Triangular Elements of Table 1

Triangle	Bending ratio r for isotropic material	$\gamma=0$ $\nu=\frac{1}{4}$	$\gamma=1$ $\nu=\frac{1}{4}$	$\gamma=4$ $\nu=\frac{1}{4}$	$\gamma=16$ $\nu=\frac{1}{4}$
ALL-3I	$\frac{584+(79-91\nu)\gamma^2+6\gamma^4}{432(1-\nu^2)}$	1.442	1.595	7.457	1007.901
ALL-3M	$\frac{24+(5-9\nu)\gamma^2+2\gamma^4}{16(1-\nu^2)}$	1.600	1.916	38.667	8786.667
ALL-EX	$\frac{84+(15-19\nu)\gamma^2+2\gamma^4}{60(1-\nu^2)}$	1.493	1.711	13.511	2378.311
ALL-LS	$\frac{1672+(263-371\nu)\gamma^2+54\gamma^4}{1200(1-\nu^2)}$	1.486	1.686	16.196	3185.956
CST	$\frac{6+3(1-\nu)\gamma^2}{2(1-\nu^2)}$	3.200	4.400	22.400	310.400
FF84	$\frac{3}{4}+\frac{13}{96(1-\nu)}+\frac{13+54\gamma^2+119\gamma^4+70\gamma^6+13\gamma^8}{96(1+3\gamma^2+\gamma^4)^2(1+\nu)}$	1.039	1.020	1.035	1.039
LST-Ret	$\frac{34+5(1-\nu)\gamma^2}{27(1-\nu^2)}$	1.343	1.491	3.714	39.269
OPT	1	1.000	1.000	1.000	1.000

5.4. Is the Optimal Element Unique?

To investigate whether the optimal element is unique, the common factor A in the matrices (28) was replaced by nine values A_{jk}, $j=1,2,3$, $k=1,2,3$. These have dimensions of area but are otherwise arbitrary. A_{jk} is assigned to the $\{j,k\}$ entry of $\mathbf{Q}_1$ and then cyclically carried through $\mathbf{Q}_2$ and $\mathbf{Q}_3$. If the energy orthogonality condition (34) is enforced *a priori*, a complete symbolic analysis of the bending ratio was possible with *Mathematica*. Except for β_0 the previous solution (41) re-emerges for $r\equiv 1$ in the sense that the $A_{jk}=A$ and the β_i are recovered except for a scaling factor. Absorbing this factor into β_0 the same element is obtained.

If the orthogonality constraint (34) is not enforced *a priori*, the energy balance conditions become highly complicated (a system of three quartic polynomial equations emerges with unknown terms $\beta_i\beta_j A_{k\ell}A_{mn}$) and no simple solution was found. Thus the question of whether non-energy-orthogonal optimal elements of this configuration exist remains open.

5.5. Morphing

Morphing means transforming an individual element or macroelement into a simpler model using kinematic constraints. Often the simpler element has lower dimensionality. For example a plate bending macroelement may be morphed to a beam or a torqued shaft [7]. To illustrate the idea consider transforming the rectangular panel of Figure 9 into the two-node Bernoulli-Euler beam-column element shown on the right of that Figure. The length, cross sectional area and moment of inertia of the beam-column element, respectively, are denoted by $L=a$, $A=bh$ and $I_{zz}=b^3h/12=a^3h/(12\gamma^3)$, respectively.

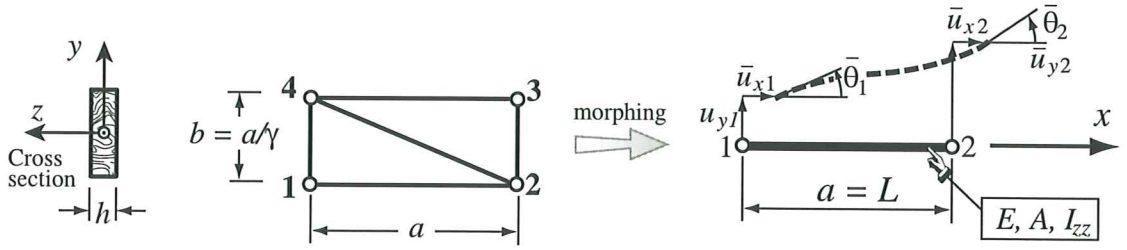

Figure 9. Morphing a 12-DOF two-triangle mesh unit to a 6-DOF beam-column element.

The transformation between the freedoms of the mesh unit and those of the beam-column is

$$\mathbf{u}_R = \begin{bmatrix} u_{x1} \\ u_{y1} \\ \theta_1 \\ u_{x2} \\ u_{y2} \\ \theta_2 \\ u_{x3} \\ u_{y3} \\ \theta_3 \\ u_{x4} \\ u_{y4} \\ \theta_4 \end{bmatrix} = \begin{bmatrix} 1 & 0 & \frac{1}{2}b & 0 & 0 & 0 \\ 0 & 1 & 0 & 0 & 0 & 0 \\ 0 & 0 & 1 & 0 & 0 & 0 \\ 0 & 0 & 0 & 1 & 0 & \frac{1}{2}b \\ 0 & 0 & 0 & 0 & 1 & 0 \\ 0 & 0 & 0 & 0 & 0 & 1 \\ 0 & 0 & 0 & 1 & 0 & -\frac{1}{2}b \\ 0 & 0 & 0 & 0 & 1 & 0 \\ 0 & 0 & 0 & 0 & 0 & 1 \\ 1 & 0 & -\frac{1}{2}b & 0 & 0 & 0 \\ 0 & 1 & 0 & 0 & 0 & 0 \\ 0 & 0 & 1 & 0 & 0 & 0 \end{bmatrix} \begin{bmatrix} \bar{u}_{x1} \\ \bar{u}_{y1} \\ \bar{\theta}_1 \\ \bar{u}_{x2} \\ \bar{u}_{y2} \\ \bar{\theta}_2 \end{bmatrix} = \mathbf{T}_m \bar{\mathbf{u}}_m. \tag{43}$$

where a superposed bar distinguishes the beam-column freedoms grouped in array $\bar{\mathbf{u}}_m$. Let $\mathbf{K}_R^{unit}$ denote the 12×12 stiffness of the mesh unit of Figure 9 assembled with two optimal LST-3/9R triangles triangles. For isotropic material with $\nu = 0$ a symbolic calculation gives the morphed stiffness

$$\mathbf{K}_m = \mathbf{T}_m^T \mathbf{K}_R^{unit} \mathbf{T}_m = \frac{E}{L} \begin{bmatrix} A & 0 & 0 & -A & 0 & 0 \\ 0 & 12c_{22}I_{zz}/L^2 & 6c_{23}I_{zz}/L & 0 & -12c_{22}I_{zz}/L^2 & 6c_{23}I_{zz}/L \\ 0 & 6c_{23}I_{zz}/L & 4c_{33}I_{zz} & 0 & -6c_{23}I_{zz}/L & 4c_{33}I_{zz} \\ -A & 0 & 0 & A & 0 & 0 \\ 0 & 12c_{22}I_{zz}/L^2 & 6c_{23}I_{zz}/L & 0 & -12c_{22}I_{zz}/L^2 & 6c_{23}I_{zz}/L \\ 0 & 6c_{23}I_{zz}/L & 4c_{33}I_{zz} & 0 & -6c_{23}I_{zz}/L & 4c_{33}I_{zz} \end{bmatrix}, \tag{44}$$

in which $c_{22} = c_{23} = (1+8\gamma^2+\gamma^4)/12$ and $c_{33} = (5+8\gamma^2+\gamma^4)/16$. The entries in rows/columns 1 and 4 form the well known two-node bar stiffness. Those in rows and columns 2, 3, 5 and 6 are dimensionally homogeneous to those of a C^1 beam, and may be grouped into the following matrix configuration:

$$\mathbf{K}_m^{beam} = \frac{EI_{zz}}{L} \left(\begin{bmatrix} 0 & 0 & 0 & 0 \\ 0 & 1 & 0 & -1 \\ 0 & 0 & 0 & 0 \\ 0 & -1 & 0 & 1 \end{bmatrix} + \bar{\beta} \begin{bmatrix} 12/L^2 & 6/L & -12/L^2 & 6/L \\ 6/L & 3 & -6/L & 3 \\ -12/L^2 & -6/L & 12/L^2 & -6/L \\ 6/L & 3 & -6/L & 3 \end{bmatrix} \right) \tag{45}$$

with $\bar{\beta} = c_{22} = c_{23} = (4c_{33} - 1)/3 = (1 + 8\gamma^2 + \gamma^4)/12$. For arbitrary Poisson's ratio, $\bar{\beta} = ((1 - 4\nu^2)(1 + \gamma^4) + \gamma^2(8 - 9\nu + 8\nu^2 - 12\nu^3))/(12(1 - \nu^2))$.

Now (45) happens to be the universal template of a prismatic beam, first presented in [38] and further studied, for the C^1 case, in [42,43] using Fourier methods. The basic stiffness on the left characterizes the pure-bending symmetric response to a uniform bending moment, whereas the higher-order stiffness on the right characterizes the antisymmetric response to a linearly-varying, bending moment of zero mean. For the C^1 Bernoulli-Euler beam constructed with cubic shape functions, $\bar{\beta} = 1$. For the C^0 Timoshenko beam, the exact equilibrium model [44, p. 80] is matched by $\bar{\beta} = 1/(1+\phi)$, $\phi = 12EI_z/(GA_sL^2)$, in which $A_s = 5bh/6$ is the shear area and $G = \frac{1}{2}E/(1+\nu)$ the shear modulus.

As γ grows the morphed beam template shows that the antisymmetric response, as scaled by $\bar{\beta}$, stiffens rapidly. However, the symmetric response is exact for any γ, which confirms the optimality of the triangular macroelement. Observe also that what was a higher order patch test on the two-triangle mesh unit becomes a basic (constant-moment) patch test on the morphed element. This is typical of morphing transformations that reduce spatial dimensionality.

What is the difference between morphing and retrofitting? They share techniques but have different goals: the morphed element is not used as a product but as a way to learn about the source element.

5.6. Strain and Stress Recovery

Once node displacements are computed, element strains and stresses can be recovered using the following scheme. Let $\mathbf{u}^e$ denote the compute node displacements. The Cartesian stresses at a point $\{\zeta_1, \zeta_2, \zeta_3\}$ are $\boldsymbol{\sigma} = \mathbf{E}\mathbf{e}$, in which the Cartesian strains are computed from

$$\mathbf{e} = (\mathbf{L}^T/(Ah)\,\mathbf{u}^e + \mathbf{T}_e\beta_0^e(\mathbf{Q}_1\zeta_1 + \mathbf{Q}_2\zeta_2 + \mathbf{Q}_3\zeta_3)\mathbf{T}_{\bar{\theta}u}\mathbf{u}^e, \tag{46}$$

Here $\mathbf{L}$ is the lumping matrix (21) computed with $\alpha_b = 3/2$, and $\mathbf{Q}_i$ are the matrices (28) computed with the optimal parameters (42). However $\beta_0^e \neq \beta_0 = (1-4\nu^2)/2$. Least square fit studies suggest using $\beta_0^e = 3/2$ instead. This value is used in the stress results reported in Sections 9ff.

6. A MATHEMATICA IMPLEMENTATION

Figure 10 lists a *Mathematica* implementation of (31) as Module `LST39RMembTemplateStiffness`. The four module arguments are the node coordinates `xycoor` ordered `{{x1,y1},{x2,y2},{x3,y3}}`, the 3×3 stress-strain matrix `Emat`, the thickness `h` and the set of free parameters ordered $\{\alpha_b, \beta_0, \beta_1, \beta_2, \ldots \beta_9\}$. The module returns matrices $\mathbf{K}_b$ and $\mathbf{K}_h$ as list `{Kb,Kh}`, a separate return of the two matrices being useful for research work.

This implementation emphasizes readibility and may be further streamlined. For example in low level coding $\mathbf{Q}_4$, $\mathbf{Q}_5$ and $\mathbf{Q}_6$ should be formed directly. A carefully coded C or Fortran implementation can form $\mathbf{K}_b + \mathbf{K}_h$ in about 500 floating point operations. On a 1-GF processor (e.g., forthcoming >3GHz Intel CPUs) that comes to over 1 million elements per second. A 18-DOF shell element using this triangle as membrane component can be formed in roughly 2000 floating point operations.

To expedite "cloning tests" suggested in the Conclusions, the optimal stiffness of a triangle with $x_1 = y_1 = 0$, $x_2 = 4.08$, $y_2 = -3.44$, $x_3 = 3.4$, $y_3 = 1.14$, $E = 120$, $\nu = 1/4$ and $h = 1/8$ is formed and displayed by the statements in Figure 11. (Module `LST39ANDESTemplateSignature` referenced therein is discussed below.) `SetPrecision` keeps output entries down to 5 significant places so matrices fit across the page. The results are

```
LST39RMembTemplateStiffness [xycoor_,Emat_,h_,fpars_]:=Module[
 {x1,y1,x2,y2,x3,y3,x12,y12,x21,y21,x23,y23,x32,y32,x31,y31,
 x13,y13,A,A4,V,LL21,LL32,LL13,αb,β0,β1,β2,β3,β4,β5,β6,β7,β8,β9,
 Te,Tθu,Q1,Q2,Q3,Q4,Q5,Q6,c,L,Enat,Kθ,Kh,Kb,Ke},
 {{x1,y1},{x2,y2},{x3,y3}}=xycoor;
 {αb,β0,β1,β2,β3,β4,β5,β6,β7,β8,β9}=fpars;
 x12=x1-x2; x23=x2-x3; x31=x3-x1; x21=-x12; x32=-x23; x13=-x31;
 y12=y1-y2; y23=y2-y3; y31=y3-y1; y21=-y12; y32=-y23; y13=-y31;
 A=(y21*x13-x21*y13)/2;  A2=2*A; A4=4*A;
 L= {{y23,0,x32},{0,x32,y23},
     {y23*(y13-y21),x32*(x31-x12),(x31*y13-x12*y21)*2}*αb/6,
     {y31,0,x13},{0,x13,y31},
     {y31*(y21-y32),x13*(x12-x23),(x12*y21-x23*y32)*2}*αb/6,
     {y12,0,x21},{0,x21,y12},
     {y12*(y32-y13),x21*(x23-x31),(x23*y32-x31*y13)*2}*αb/6}*h/2;
 Kb=(L.Emat.Transpose[L])/(h*A);
 Tθu={{x32,y32,A4,x13,y13, 0,x21,y21, 0},
      {x32,y32, 0,x13,y13,A4,x21,y21, 0},
      {x32,y32, 0,x13,y13, 0,x21,y21,A4}}/A4;
 LL21=x21^2+y21^2; LL32=x32^2+y32^2; LL13=x13^2+y13^2;
 Te={{y23*y13*LL21,   y31*y21*LL32,   y12*y32*LL13},
     {x23*x13*LL21,   x31*x21*LL32,   x12*x32*LL13},
     {(y23*x31+x32*y13)*LL21,(y31*x12+x13*y21)*LL32,
      (y12*x23+x21*y32)*LL13}}/(A*A4);
 Q1={{β1,β2,β3}/LL21,{β4,β5,β6}/LL32,{β7,β8,β9}/LL13}*A2/3;
 Q2={{β9,β7,β8}/LL21,{β3,β1,β2}/LL32,{β6,β4,β5}/LL13}*A2/3;
 Q3={{β5,β6,β4}/LL21,{β8,β9,β7}/LL32,{β2,β3,β1}/LL13}*A2/3;
 Q4=(Q1+Q2)/2; Q5=(Q2+Q3)/2; Q6=(Q3+Q1)/2;
 Enat=Transpose[Te].Emat.Te;
 Kθ=(3/4)*β0*h*A*(Transpose[Q4].Enat.Q4+Transpose[Q5].Enat.Q5+
                  Transpose[Q6].Enat.Q6);
 Kh=Transpose[Tθu].Kθ.Tθu;
 Return[{Kb,Kh}]];
```

Figure 10. A Mathematica implementation of the LST-3/9R ANDES template (31).

$$\mathbf{K}_b = \begin{bmatrix} 10.350 & 0.95258 & 7.7327 & -2.1309 & 1.7629 & 2.1745 & -8.2194 & -2.7155 & -9.9073 \\ 0.95258 & 4.0758 & 8.1695 & 2.7629 & 0.17327 & -5.7458 & -3.7155 & -4.2491 & -2.4237 \\ 7.7327 & 8.1695 & 19.723 & 3.9414 & 1.3377 & -9.4943 & -11.674 & -9.5072 & -10.229 \\ -2.1309 & 2.7629 & 3.9414 & 2.7575 & -1.1855 & -4.1179 & -0.62660 & -1.5774 & 0.17657 \\ 1.7629 & 0.17327 & 1.3377 & -1.1855 & 5.8957 & -4.6390 & -0.57737 & -6.0690 & 3.3013 \\ 2.1745 & -5.7458 & -9.4943 & -4.1179 & -4.6390 & 13.777 & 1.9434 & 10.385 & -4.2825 \\ -8.2194 & -3.7155 & -11.674 & -0.62660 & -0.57737 & 1.9434 & 8.8460 & 4.2928 & 9.7307 \\ -2.7155 & -4.2491 & -9.5072 & -1.5774 & -6.0690 & 10.385 & 4.2928 & 10.318 & -0.87754 \\ -9.9073 & -2.4237 & -10.229 & 0.17657 & 3.3013 & -4.2825 & 9.7307 & -0.87754 & 14.512 \end{bmatrix} \tag{47}$$

$$\mathbf{K}_h = \begin{bmatrix} 0.041538 & -0.27977 & -0.63728 & 0.20769 & 0.069638 & -0.52781 & -0.24923 & 0.21014 & -0.83208 \\ -0.27977 & 1.8844 & 4.2923 & -1.3989 & -0.46903 & 3.5549 & 1.6786 & -1.4153 & 5.6043 \\ -0.63728 & 4.2923 & 12.833 & -3.1864 & -1.0684 & 7.7151 & 3.8237 & -3.2239 & 10.092 \\ 0.20769 & -1.3989 & -3.1864 & 1.0385 & 0.34819 & -2.6390 & -1.2462 & 1.0507 & -4.1604 \\ 0.069638 & -0.46903 & -1.0684 & 0.34819 & 0.11675 & -0.88485 & -0.41783 & 0.35229 & -1.3950 \\ -0.52781 & 3.5549 & 7.7151 & -2.6390 & -0.88485 & 7.9515 & 3.1668 & -2.6701 & 9.7104 \\ -0.24923 & 1.6786 & 3.8237 & -1.2462 & -0.41783 & 3.1668 & 1.4954 & -1.2608 & 4.9925 \\ 0.21014 & -1.4153 & -3.2239 & 1.0507 & 0.35229 & -2.6701 & -1.2608 & 1.0630 & -4.2093 \\ -0.83208 & 5.6043 & 10.092 & -4.1604 & -1.3950 & 9.7104 & 4.9925 & -4.2093 & 20.204 \end{bmatrix} \tag{48}$$

```
xycoor=N[{{0,0},{102/25,-86/25},{85/25,285/250}}];
Print["xycoor=",xycoor];
Em=120; ν=1/4; h=1/8;
Emat=Em/(1-ν^2)*{{1,ν,0},{ν,1,0},{0,0,(1-ν)/2}};
fpars= LST39RANDESTemplateSignature["OPT",ν];
{Kb,Kh}=LST39RMembTemplateStiffness [xycoor,Emat,h,fpars];
Print["Kb=",SetPrecision[N[Kb],5]//MatrixForm];
Print["Kh=",SetPrecision[N[Kh],5]//MatrixForm];
Print["Ke=",SetPrecision[N[Kb+Kh],5]//MatrixForm];
Print["eigs of Ke=",Chop[Eigenvalues[N[Kb+Kh]]]];
```

Figure 11. Test statements that produce the matrices (47)–(49).

```
LST39RANDESTemplateSignature[name_,nu_]:=Module[{fpars},
    fpars={0,0,0,0,0,0,0,0,0,0,0}; (* CST *)
    If [name=="OPT",
        fpars={3/2,Max[(1-4*nu^2)/2,1/100],1,2,1,0,1,-1,-1,-1,-2}];
    If [name=="ALL3I",
        fpars={ 1,4/9,1/12,5/12,1/2,0,1/3,-1/3,-1/12,-1/2,-5/12}];
    If [name=="ALL3M",
        fpars={ 1,4/9,1/4,5/4,3/2,0,1,-1,-1/4,-3/2,-5/4}];
    If [name=="ALLLS",
        fpars={ 1,4/9,3/20,3/4,9/10,0,3/5,-3/5,-3/20,-9/10,-3/4}];
    If [name=="LSTRet",
        fpars={4/3,1/2,2/3,-2/3,0,0,-4/3,4/3,-2/3,0,2/3}];
    Return[fpars]];
```

Figure 12. Module to return signature given a template instance name.

$$\mathbf{K}_R = \mathbf{K}_b + \mathbf{K}_h =$$

$$\begin{bmatrix}
10.392 & 0.67281 & 7.0955 & -1.9232 & 1.8325 & 1.6467 & -8.4687 & -2.5053 & -10.739 \\
0.67281 & 5.9602 & 12.462 & 1.3640 & -0.29577 & -2.1909 & -2.0368 & -5.6644 & 3.1805 \\
7.0955 & 12.462 & 32.557 & 0.75498 & 0.26929 & -1.7792 & -7.8504 & -12.731 & -0.13702 \\
-1.9232 & 1.3640 & 0.75498 & 3.7959 & -0.83734 & -6.7570 & -1.8728 & -0.52670 & -3.9838 \\
1.8325 & -0.29577 & 0.26929 & -0.83734 & 6.0125 & -5.5238 & -0.99520 & -5.7167 & 1.9063 \\
1.6467 & -2.1909 & -1.7792 & -6.7570 & -5.5238 & 21.728 & 5.1102 & 7.7147 & 5.4278 \\
-8.4687 & -2.0368 & -7.8504 & -1.8728 & -0.99520 & 5.1102 & 10.341 & 3.0320 & 14.723 \\
-2.5053 & -5.6644 & -12.731 & -0.52670 & -5.7167 & 7.7147 & 3.0320 & 11.381 & -5.0869 \\
-10.739 & 3.1805 & -0.13702 & -3.9838 & 1.9063 & 5.4278 & 14.723 & -5.0869 & 34.716
\end{bmatrix} \tag{49}$$

The eigenvalues of $\mathbf{K}_R$ to 5 places are [52.913 43.834 26.434 11.181 1.8722 0.64900 0 0 0].

When doing element comparison studies as in Section 9 it is convenient to pass from a user supplied mnemonic name to the set of free parameters (template signature). Module `LST39ANDESTemplateSignature`, listed in Figure 12, returns the template signature given an mnemonic type name. For example `LST39ANDESTemplateSignature["LSTRet",0]` returns {4/3, 1/2, 2/3, −2/3, 0, 0, −4/3, 4/3, −2/3, 0, 2/3} as the set of free parameters for the retrofitted LST derived in Section 7.

7. RETROFITTING LST

The process of building templates by direct fabrication may look like black magic to the uninitiated. By comparison, retrofitting a well known "parent" element appears straightforward because kinematic constraints and congruential transformations are taught in introductory FEM courses.

7.1. Midpoint Migration Migraines

The idea explored in this section is to start with the conventional Linear Strain Triangle depicted in Figure 3(a). The LST-3/12C has 12 DOFs arranged as

$$\mathbf{u}_C = [\, u_{x1} \;\; u_{y1} \;\; u_{x2} \;\; u_{y2} \;\; u_{x3} \;\; u_{y3} \;\; u_{x4} \;\; u_{y4} \;\; u_{x5} \;\; u_{y5} \;\; u_{x6} \;\; u_{y6} \,]^T \,. \tag{50}$$

The triangle has straight sides, with nodes 4, 5 and 6 at the midpoints. (It makes no sense to start with the more general curved-side iso-P element since these nodes are eventually eliminated.) The stiffness of this superparametric triangle is readily computed in closed form since the Jacobian is constant. For constant $\mathbf{E}$ and h, a very simple expression, discovered in 1966 [12], is

$$\mathbf{K}_C = \tfrac{1}{3} A h \left(\mathbf{B}_1^T \mathbf{E} \mathbf{B}_1 + \mathbf{B}_2^T \mathbf{E} \mathbf{B}_2 + \mathbf{B}_3^T \mathbf{E} \mathbf{B}_3 \right) \tag{51}$$

in which A is the triangle area and

$$\begin{aligned}
\mathbf{B}_1 &= \frac{1}{2A} \begin{bmatrix} y_{32} & 0 & y_{31} & 0 & y_{12} & 0 & 2y_{23} & 0 & 2y_{32} & 0 & 2y_{23} & 0 \\ 0 & x_{23} & 0 & x_{13} & 0 & x_{21} & 0 & 2x_{32} & 0 & 2x_{23} & 0 & 2x_{32} \\ x_{23} & y_{32} & x_{13} & y_{31} & x_{21} & y_{12} & 2x_{32} & 2y_{23} & 2x_{23} & 2y_{32} & 2x_{32} & 2y_{23} \end{bmatrix} \\
\mathbf{B}_2 &= \frac{1}{2A} \begin{bmatrix} y_{23} & 0 & y_{13} & 0 & y_{12} & 0 & 2y_{31} & 0 & 2y_{31} & 0 & 2y_{13} & 0 \\ 0 & x_{32} & 0 & x_{31} & 0 & x_{21} & 0 & 2x_{13} & 0 & 2x_{13} & 0 & 2x_{31} \\ x_{32} & y_{23} & x_{31} & y_{13} & x_{21} & y_{12} & 2x_{13} & 2y_{31} & 2x_{13} & 2y_{31} & 2x_{31} & 2y_{13} \end{bmatrix} \\
\mathbf{B}_3 &= \frac{1}{2A} \begin{bmatrix} y_{23} & 0 & y_{31} & 0 & y_{21} & 0 & 2y_{21} & 0 & 2y_{12} & 0 & 2y_{12} & 0 \\ 0 & x_{32} & 0 & x_{13} & 0 & x_{12} & 0 & 2x_{12} & 0 & 2x_{21} & 0 & 2x_{21} \\ x_{32} & y_{23} & x_{13} & y_{31} & x_{12} & y_{21} & 2x_{12} & 2y_{21} & 2x_{21} & 2y_{12} & 2x_{21} & 2y_{12} \end{bmatrix}
\end{aligned} \tag{52}$$

Next, establish by some method a "midpoint migration" 12×9 transformation matrix $\mathbf{T}_{CR}$ that links $\mathbf{u}_C = \mathbf{T}_{CR} \mathbf{u}_R$, where the latter is configured as per (12). Then the LST-3/9R stiffness is

$$\mathbf{K}_L = \mathbf{T}_{CR}^T \mathbf{K}_C \mathbf{T}_{CR} \tag{53}$$

where the subscript distinguishes this stiffness from that derived in the previous section. One advantage of this technique is that $\mathbf{T}_{CR}$ can be reused to produce consistent mass, geometric stiffness matrices and consistent forces from those of the LST-6/12C, which are well known and available in many codes.

If this sounds too good to be true, it is. Three things may go wrong. First, there is no guarantee that (53) will pass the patch test. Generally it will not: as shown below, the $\mathbf{T}_{CR}$ form that does it while avoiding the second problem is very special. Second, the transformation may "blow up" for some triangle geometries. Third, the element may be rank deficient.

There are no easy fix-up cures for any of these mishaps. Repeated failures during the 1970s prompted Irons and Ahmad in 1980 to proclaim, a bit prematurely, that trying to construct membrane elements with drilling freedoms was a waste of time [45, p. 289]. To be fair, some of the tools used here were not known at the time. In particular the fundamental decomposition (17), which facilitates passing the patch test *a priori*, came after their book.

7.2. Divide and Conquer

Begin by decomposing the stiffness $\mathbf{K}_C$ of (51) into basic and higher order: $\mathbf{K}_C = \mathbf{K}_{Cb} + \mathbf{K}_{Ch}$. It is easily checked that for constant $\mathbf{E}$ and h

$$\mathbf{K}_{Cb} = A\,h\,\mathbf{B}_0^T\,\mathbf{E}\,\mathbf{B}_0, \qquad \mathbf{K}_{Ch} = \tfrac{1}{3}A\,h\,\big(\mathbf{B}_{h1}^T\,\mathbf{E}\,\mathbf{B}_{h1} + \mathbf{B}_{h2}^T\,\mathbf{E}\,\mathbf{B}_{h2} + \mathbf{B}_{h3}^T\,\mathbf{E}\,\mathbf{B}_{h3}\big). \tag{54}$$

in which $\mathbf{B}_0 = \frac{1}{3}(\mathbf{B}_1 + \mathbf{B}_2 + \mathbf{B}_3)$ and $\mathbf{B}_{hi} = \mathbf{B}_i - \mathbf{B}_0$, $i = 1, 2, 3$. Explicit forms of the strain-displacement matrices are

$$\mathbf{B}_0 = \frac{1}{6A}\begin{bmatrix} y_{23} & 0 & y_{31} & 0 & y_{12} & 0 & 4y_{21} & 0 & 4y_{32} & 0 & 4y_{13} & 0 \\ 0 & x_{32} & 0 & x_{13} & 0 & x_{21} & 0 & 4x_{12} & 0 & 4x_{23} & 0 & 4x_{31} \\ x_{32} & y_{23} & x_{13} & y_{31} & x_{21} & y_{12} & 4x_{12} & 4y_{21} & 4x_{23} & 4y_{32} & 4x_{31} & 4y_{13} \end{bmatrix}$$

$$\mathbf{B}_{h1} = \frac{1}{3A}\begin{bmatrix} 2y_{32} & 0 & y_{31} & 0 & y_{12} & 0 & 2y_{13}{+}y_{23} & 0 & y_{32} & 0 & 2y_{21}{+}y_{23} & 0 \\ 0 & 2x_{23} & 0 & x_{13} & 0 & x_{21} & 0 & x_{13}{+}2x_{23} & 0 & x_{23} & 0 & 2x_{12}{+}x_{32} \\ 2x_{23} & 2y_{32} & x_{13} & y_{31} & x_{21} & y_{12} & x_{13}{+}2x_{23} & 2y_{13}{+}y_{23} & x_{23} & y_{32} & 2x_{12}{+}x_{32} & 2y_{21}{+}y_{23} \end{bmatrix}$$

$$\mathbf{B}_{h2} = \frac{1}{3A}\begin{bmatrix} y_{23} & 0 & 2y_{13} & 0 & y_{12} & 0 & y_{31}{+}2y_{32} & 0 & 2y_{21}{+}y_{31} & 0 & y_{13} & 0 \\ 0 & x_{32} & 0 & 2x_{31} & 0 & x_{21} & 0 & x_{13}{+}2x_{23} & 0 & 2x_{12}{+}x_{13} & 0 & x_{31} \\ x_{32} & y_{23} & 2x_{31} & 2y_{13} & x_{21} & y_{12} & x_{13}{+}2x_{23} & y_{31}{+}2y_{32} & 2x_{12}{+}x_{13} & 2y_{21}{+}y_{31} & x_{31} & y_{13} \end{bmatrix}$$

$$\mathbf{B}_{h3} = \frac{1}{3A}\begin{bmatrix} y_{23} & 0 & y_{31} & 0 & 2y_{21} & 0 & y_{21} & 0 & 2y_3{+}y_{12} & 0 & y_{12}{+}2y_{32} & 0 \\ 0 & x_{32} & 0 & x_{13} & 0 & 2x_{12} & 0 & x_{12} & 0 & x_{21}{+}2x_{31} & 0 & x_{21}{+}2x_{23} \\ x_{32} & y_{23} & x_{13} & y_{31} & 2x_{12} & 2y_{21} & x_{12} & y_{21} & x_{21}{+}2x_{31} & 2y_3{+}y_{12} & x_{21}{+}2x_{23} & y_{12}{+}2y_{32} \end{bmatrix} \tag{55}$$

While $\mathbf{B}_0$ is unique, there are several $\mathbf{B}_{hi}$ matrices that produce the same $\mathbf{K}_{Ch}$ through the formula in (54). This indeterminacy causes no problems, however, since $\mathbf{K}_{Ch}$ is unique because $\mathbf{K}_C$ and $\mathbf{K}_{Cb}$ are. Insertion of $\mathbf{K}_C = \mathbf{K}_{Cb} + \mathbf{K}_{Ch}$ into (53) shows that

$$\mathbf{K}_L = \mathbf{K}_{Lb} + \mathbf{K}_{Lh}, \qquad \mathbf{K}_{Lb} = \mathbf{T}_{CR}^T\mathbf{K}_{Cb}\mathbf{T}_{CR}, \qquad \mathbf{K}_{Lh} = \mathbf{T}_{CR}^T\mathbf{K}_{Ch}\mathbf{T}_{CR}. \tag{56}$$

Next, we make use of the hierarchical form of the LST introduced in [46, p. 222]. This variant, labelled LST-6/20CH, has the same nodes as the LST-6/12C but the midpoint freedoms are deviations from linearity:

$$\tilde{\mathbf{u}}_C = [\,u_{x1}\;\; u_{y1}\;\; u_{x2}\;\; u_{y2}\;\; u_{x3}\;\; u_{y3}\;\; \tilde{u}_{x4}\;\; \tilde{u}_{y4}\;\; \tilde{u}_{x5}\;\; \tilde{u}_{y5}\;\; \tilde{u}_{x6}\;\; \tilde{u}_{y6}\,]^T. \tag{57}$$

where $\tilde{u}_{x4} = u_{x4} - \frac{1}{2}(u_{x1} + u_{x2})$, $\tilde{u}_{y4} = u_{y4} - \frac{1}{2}(u_{y1} + u_{y2})$, etc. The freedoms of the conventional and hierarchical LST are related by the transformation

$$\mathbf{u}_C = \mathbf{T}_{CH}\,\tilde{\mathbf{u}}_C, \qquad \tilde{\mathbf{u}}_C = \mathbf{T}_{HC}\,\mathbf{u}_C, \tag{58}$$

in which

$$\mathbf{T}_{CH} = \begin{bmatrix} 1 & 0 & 0 & 0 & 0 & 0 & 0 & 0 & 0 & 0 & 0 & 0 \\ 0 & 1 & 0 & 0 & 0 & 0 & 0 & 0 & 0 & 0 & 0 & 0 \\ 0 & 0 & 1 & 0 & 0 & 0 & 0 & 0 & 0 & 0 & 0 & 0 \\ 0 & 0 & 0 & 1 & 0 & 0 & 0 & 0 & 0 & 0 & 0 & 0 \\ 0 & 0 & 0 & 0 & 1 & 0 & 0 & 0 & 0 & 0 & 0 & 0 \\ 0 & 0 & 0 & 0 & 0 & 1 & 0 & 0 & 0 & 0 & 0 & 0 \\ \frac{1}{2} & 0 & \frac{1}{2} & 0 & 0 & 0 & 1 & 0 & 0 & 0 & 0 & 0 \\ 0 & \frac{1}{2} & 0 & \frac{1}{2} & 0 & 0 & 0 & 1 & 0 & 0 & 0 & 0 \\ 0 & 0 & \frac{1}{2} & 0 & \frac{1}{2} & 0 & 0 & 0 & 1 & 0 & 0 & 0 \\ 0 & 0 & 0 & \frac{1}{2} & 0 & \frac{1}{2} & 0 & 0 & 0 & 1 & 0 & 0 \\ \frac{1}{2} & 0 & 0 & 0 & \frac{1}{2} & 0 & 0 & 0 & 0 & 0 & 1 & 0 \\ 0 & \frac{1}{2} & 0 & 0 & 0 & \frac{1}{2} & 0 & 0 & 0 & 0 & 0 & 1 \end{bmatrix} \tag{59}$$

The inverse $\mathbf{T}_{HC} = \mathbf{T}_{CH}^{-1}$ is obtained by changing all $\frac{1}{2}$ to $-\frac{1}{2}$. It follows that

$$\tilde{\mathbf{K}}_C = \mathbf{T}_{HC}^T \mathbf{K}_C \mathbf{T}_{HC} = \tilde{\mathbf{K}}_{Cb} + \tilde{\mathbf{K}}_{Ch}, \quad \tilde{\mathbf{K}}_{Cb} = \mathbf{T}_{HC}^T \mathbf{K}_{Cb} \mathbf{T}_{HC}, \quad \tilde{\mathbf{K}}_{Ch} = \mathbf{T}_{HC}^T \mathbf{K}_{Ch} \mathbf{T}_{HC}. \tag{60}$$

From the Free Formulation let us borrow a couple of modal-basis matrices:

$$\mathbf{G}_{Cb} = \begin{bmatrix} 1 & 0 & y_1 & x_1 & 0 & y_1 \\ 0 & 1 & -x_1 & 0 & y_1 & x_1 \\ 1 & 0 & y_2 & x_2 & 0 & y_2 \\ 0 & 1 & -x_2 & 0 & y_2 & x_2 \\ 1 & 0 & y_3 & x_3 & 0 & y_3 \\ 0 & 1 & -x_3 & 0 & y_3 & x_3 \\ 1 & 0 & y_4 & x_4 & 0 & y_4 \\ 0 & 1 & -x_4 & 0 & y_4 & x_4 \\ 1 & 0 & y_5 & x_5 & 0 & y_5 \\ 0 & 1 & -x_5 & 0 & y_5 & x_5 \\ 1 & 0 & y_6 & x_6 & 0 & y_6 \\ 0 & 1 & -x_6 & 0 & y_6 & x_6 \end{bmatrix}, \quad \mathbf{G}_{Rb} = \begin{bmatrix} 1 & 0 & y_1 & x_1 & 0 & y_1 \\ 0 & 1 & -x_1 & 0 & y_1 & x_1 \\ 0 & 0 & 1 & 0 & 0 & 0 \\ 1 & 0 & y_2 & x_2 & 0 & y_2 \\ 0 & 1 & -x_2 & 0 & y_2 & x_2 \\ 0 & 0 & 1 & 0 & 0 & 0 \\ 1 & 0 & y_3 & x_3 & 0 & y_3 \\ 0 & 1 & -x_3 & 0 & y_3 & x_3 \\ 0 & 0 & 1 & 0 & 0 & 0 \end{bmatrix} \tag{61}$$

and their hierarchical counterparts:

$$\tilde{\mathbf{G}}_{Cb} = \mathbf{G}_{Cb}\mathbf{T}_{CR} = \begin{bmatrix} 1 & 0 & y_1 & x_1 & 0 & y_1 \\ 0 & 1 & -x_1 & 0 & y_1 & x_1 \\ 1 & 0 & y_2 & x_2 & 0 & y_2 \\ 0 & 1 & -x_2 & 0 & y_2 & x_2 \\ 1 & 0 & y_3 & x_3 & 0 & y_3 \\ 0 & 1 & -x_3 & 0 & y_3 & x_3 \\ 0 & 0 & 0 & 0 & 0 & 0 \\ 0 & 0 & 0 & 0 & 0 & 0 \\ 0 & 0 & 0 & 0 & 0 & 0 \\ 0 & 0 & 0 & 0 & 0 & 0 \\ 0 & 0 & 0 & 0 & 0 & 0 \\ 0 & 0 & 0 & 0 & 0 & 0 \end{bmatrix}, \quad \tilde{\mathbf{G}}_{Rb} = \mathbf{G}_{Rb}\mathbf{T}_{u\tilde{u}} = \begin{bmatrix} 1 & 0 & y_1 & x_1 & 0 & y_1 \\ 0 & 1 & -x_1 & 0 & y_1 & x_1 \\ 0 & 0 & 0 & 0 & 0 & 0 \\ 1 & 0 & y_2 & x_2 & 0 & y_2 \\ 0 & 1 & -x_2 & 0 & y_2 & x_2 \\ 0 & 0 & 0 & 0 & 0 & 0 \\ 1 & 0 & y_3 & x_3 & 0 & y_3 \\ 0 & 1 & -x_3 & 0 & y_3 & x_3 \\ 0 & 0 & 0 & 0 & 0 & 0 \end{bmatrix} \tag{62}$$

The first three columns of each matrix span the rigid body modes and the last three the constant strain modes evaluated at the nodes (these bases are not orthonormalized since that property is not required here.) Collectively these six columns are called the basic kinematic modes, hence the subscript.

The hierarchical form of $\mathbf{T}_{CR}$ is $\tilde{\mathbf{T}}_{CR}$, connecting $\tilde{\mathbf{K}}_L = \tilde{\mathbf{T}}_{CR}^T \mathbf{K}_R \tilde{\mathbf{T}}_{CR}$. This 12×9 matrix has 108 entries. But 90 are immediately set to 1 or 0 by the obvious assumption: the hierarchical rotations $\tilde{\theta}_i$, $i = 1, 2, 3$ are defined only by the hierarchical midpoint displacements $\tilde{u}_{xm}$, $\tilde{u}_{ym}$, $m = 4, 5, 6$. Consequently $\tilde{\mathbf{T}}_{CR}$ must have the form

$$\tilde{\mathbf{T}}_{CR} = \begin{bmatrix} 1 & 0 & 0 & 0 & 0 & 0 & 0 & 0 & 0 \\ 0 & 1 & 0 & 0 & 0 & 0 & 0 & 0 & 0 \\ 0 & 0 & 0 & 1 & 0 & 0 & 0 & 0 & 0 \\ 0 & 0 & 0 & 0 & 1 & 0 & 0 & 0 & 0 \\ 0 & 0 & 0 & 0 & 0 & 0 & 1 & 0 & 0 \\ 0 & 0 & 0 & 0 & 0 & 0 & 0 & 1 & 0 \\ 0 & 0 & q_{12} & 0 & 0 & q_{21} & 0 & 0 & q_{33} \\ 0 & 0 & p_{21} & 0 & 0 & p_{12} & 0 & 0 & p_{33} \\ 0 & 0 & q_{11} & 0 & 0 & q_{23} & 0 & 0 & q_{32} \\ 0 & 0 & q_{11} & 0 & 0 & p_{32} & 0 & 0 & p_{23} \\ 0 & 0 & q_{13} & 0 & 0 & q_{22} & 0 & 0 & q_{31} \\ 0 & 0 & p_{31} & 0 & 0 & p_{22} & 0 & 0 & p_{13} \end{bmatrix} \tag{63}$$

Here p_{ij} and q_{ij} are 18 undetermined coefficients with dimension of length. Now $\tilde{\mathbf{T}}_{CR}$ must preserve rigid body modes and constant strain states in the hierarchical elements. This requirement is expressed as

$$\tilde{\mathbf{G}}_{Cb} = \tilde{\mathbf{T}}_{CR} \tilde{\mathbf{G}}_{Rb} \tag{64}$$

which gives six nontrivial conditions. These are satisfied by taking $q_{11} = -(q_{23} + q_{32})$, $p_{11} = -(p_{23}+p_{32})$, $q_{22} = -(q_{13}+q_{31})$, $p_{22} = -(p_{13}+p_{31})$, $q_{33} = -(q_{12}+q_{21})$ and $p_{33} = -(p_{12}+p_{21})$. Transforming to non-hierarchical freedoms gives $\mathbf{T}_{CR} = \mathbf{T}_{HC} \tilde{\mathbf{T}}_{CR}$. Matrix $\mathbf{T}_{CR}$ gains twelve $\frac{1}{2}$ entries at midpoint locations but still has 12 undetermined coefficients.

Finally, require that the Individual Element Test (IET) be passed by forcing the basic stiffness matrices to coalesce: $\mathbf{T}_{RC}^T \mathbf{K}_{Cb} \mathbf{T}_{RC} = V\, \mathbf{T}_{RC}^T \mathbf{B}_0^T \mathbf{E} \mathbf{B}_0 \mathbf{T}_{RC} = V^{-1} \mathbf{L} \mathbf{E} \mathbf{L}^T$. Hence $V\, \mathbf{B}_0 \mathbf{T}_{RC} = \mathbf{L}^T$, where $\mathbf{L}$ is given in equation (21). The solution for p_{ij} and q_{ij} contain divisors that can vanish for certain triangular geometries unless one sets $p_{21} = -p_{12}$, $q_{21} = -q_{12}$, $p_{32} = -p_{23}$, $q_{32} = -q_{23}$, $p_{31} = -p_{13}$ and $q_{31} = -q_{13}$, whence $p_{11} = q_{11} = p_{22} = q_{22} = p_{33} = q_{33} = 0$. On doing that the unique solution is found to be $p_{12} = \frac{1}{8}\alpha_b x_{12}$, $p23 = \frac{1}{8}\alpha_b x_{23}$, $p_{13} = \frac{1}{8}\alpha_b x_{13}$, $q_{12} = \frac{1}{8}\alpha_b y_{12}$, $q_{13} = \frac{1}{8}\alpha_b y_{13}$, $q_{23} = \frac{1}{8}\alpha_b y_{23}$. Hence the only transformation that avoids singularities while

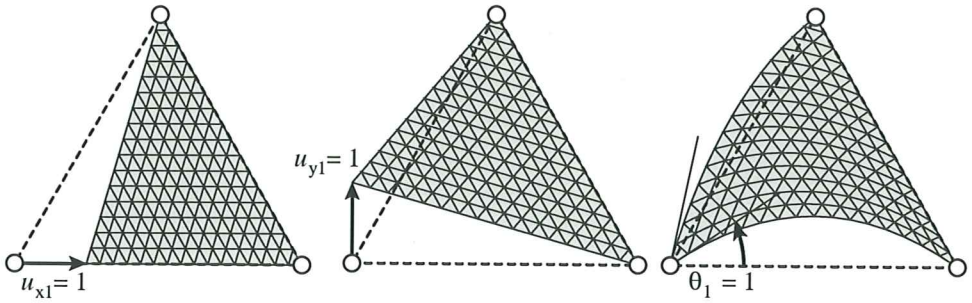

Figure 13. Shape functions for corner 1 of retrofitted LST, $\alpha_b = 1$.

satisfying the IET is

$$\mathbf{T}_{CR} = \begin{bmatrix} 1 & 0 & 0 & 0 & 0 & 0 & 0 & 0 & 0 \\ 0 & 1 & 0 & 0 & 0 & 0 & 0 & 0 & 0 \\ 0 & 0 & 0 & 1 & 0 & 0 & 0 & 0 & 0 \\ 0 & 0 & 0 & 0 & 1 & 0 & 0 & 0 & 0 \\ 0 & 0 & 0 & 0 & 0 & 0 & 1 & 0 & 0 \\ 0 & 0 & 0 & 0 & 0 & 0 & 0 & 1 & 0 \\ \frac{1}{2} & 0 & \frac{1}{8}\alpha_b y_{12} & 0 & 0 & \frac{1}{8}\alpha_b y_{21} & \frac{1}{2} & 0 & 0 \\ 0 & \frac{1}{2} & \frac{1}{8}\alpha_b x_{21} & 0 & 0 & \frac{1}{8}\alpha_b x_{12} & 0 & \frac{1}{2} & 0 \\ 0 & 0 & 0 & \frac{1}{2} & 0 & \frac{1}{8}\alpha_b y_{23} & \frac{1}{2} & 0 & \frac{1}{8}\alpha_b y_{32} \\ 0 & 0 & 0 & 0 & \frac{1}{2} & \frac{1}{8}\alpha_b x_{32} & 0 & \frac{1}{2} & \frac{1}{8}\alpha_b x_{23} \\ \frac{1}{2} & 0 & \frac{1}{8}\alpha_b y_{13} & 0 & 0 & 0 & \frac{1}{2} & 0 & \frac{1}{8}\alpha_b y_{31} \\ 0 & \frac{1}{2} & \frac{1}{8}\alpha_b x_{31} & 0 & 0 & 0 & 0 & \frac{1}{2} & \frac{1}{8}\alpha_b x_{13} \end{bmatrix} \tag{65}$$

By inspection, if $\alpha_b \neq 0$ this matrix has the nontrivial null vector:

$$\mathbf{T}\mathbf{u}_R^{null} = \mathbf{0}, \quad \mathbf{u}_R^{null} = [\,0 \;\; 0 \;\; 1 \;\; 0 \;\; 0 \;\; 1 \;\; 0 \;\; 0 \;\; 1\,]^T . \tag{66}$$

If $\alpha_b = 0$ the dimension of the null space grows to three.

The shape functions of this element are obtained on postmultiplying the shape functions of the LST-6/12 by $\mathbf{T}_{CR}$. The interpolation is

$$\begin{aligned} u_x &= N_{xx1}u_{x1} + N_{xy2}u_{y1} + N_{x\theta 1}\theta_1 + \ldots + N_{x\theta 3}\theta_3, \\ u_y &= N_{yx1}u_{x1} + N_{yy2}u_{y1} + N_{y\theta 1}\theta_1 + \ldots + N_{y\theta 3}\theta_3. \end{aligned} \tag{67}$$

where $N_{xxi} = N_{yyi} = \zeta_i\,(i = 1, 2, 3)$, $N_{xyi} = N_{yxi} = 0\,(i = 1, 2, 3)$, $N_{x\theta 1} = \alpha\zeta_1(y_{12}\zeta_2 - y_{31}\zeta_3)/2$, $N_{x\theta 2} = \alpha\zeta_2(y_{23}\zeta_3 - y_{12}\zeta_1)/2$, $N_{x\theta 3} = \alpha\zeta_3(y_{31}\zeta_1 - y_{23}\zeta_2)/2$ $N_{y\theta 1} = \alpha\zeta_1(x_{21}\zeta_2 - x_{13}\zeta_3)/2$, $N_{y\theta 1} = \alpha\zeta_2(x_{32}\zeta_3 - x_{21}\zeta_1)/2$, $N_{y\theta 1} = \alpha\zeta_3(x_{13}\zeta_1 - x_{32}\zeta_2)/2$. The shape functions for the three freedoms of corner node 1 are plotted in Figure 13. Note that the translational node displacement shape functions are the same as those of the CST-3/6C, and thus conforming. The shape functions for the rotational freedoms are quadratic and nonconforming.

7.3. Stiffness Matrix Assessment

It is easily verified that $\mathbf{K}_L$ is an instance of the ANDES template (31), with

$$\alpha_b = \alpha,\ \beta_0 = \tfrac{1}{2},\ \beta_1 = \beta_9 = \tfrac{1}{2}\alpha,\ \beta_2 = \beta_7 = -\beta_1,\ \beta_3 = \beta_4 = \beta_8 = 0,\ \beta_5 = -\alpha,\ \beta_6 = \alpha. \tag{68}$$

Computing the bending energy ratio gives for an isotropic material

$$r = c_0 + c_2\gamma^2, \quad \text{with} \quad c_0 = \frac{144 - 96\alpha_b + 25\alpha_b^2}{48(1-\nu^2)}, \quad c_2 = \frac{144 - 192\alpha_b + 73\alpha_b^2}{96(1+\nu)}. \tag{69}$$

The α_b roots of $c_2 = 0$ are imaginary, so the element cannot be bending optimal. However, the dependence of r on γ is fairly mild compared to that of the elements with $c_4 \neq 0$. Coefficient c_2 is minimized by taking $\alpha_b = 96/73 = 1.31507\ldots \approx 4/3$.

Because of (66) the element is rank deficient by one for all $\alpha_b > 0$ with $\mathbf{u}_R^{null}$ as spurious mode. This can be cured by adding the torsional mode of Figure 7 as stabilization mode. This stabilization leads to the cubic elements studied in the next Section. The bad news is that stabilization worsens significantly the aspect ratio locking.

7.4. Deriving a Mass Matrix

An advantage previously noted for the retrofitting approach is that it readily produces mass matrices, geometric stiffness matrices and consistent load vectors from those of the parent element. We give here an application of this approach for deriving a mass matrix. The consistent mass matrix of a LST-6/12C triangle of uniform thickness and mass density ρ is

$$\mathbf{M}_C = \frac{hA\rho}{180}\begin{bmatrix} 6 & 0 & -1 & 0 & -1 & 0 & 0 & 0 & -4 & 0 & 0 & 0 \\ 0 & 6 & 0 & -1 & 0 & -1 & 0 & 0 & 0 & -4 & 0 & 0 \\ -1 & 0 & 6 & 0 & -1 & 0 & 0 & 0 & 0 & 0 & -4 & 0 \\ 0 & -1 & 0 & 6 & 0 & -1 & 0 & 0 & 0 & 0 & 0 & -4 \\ -1 & 0 & -1 & 0 & 6 & 0 & -4 & 0 & 0 & 0 & 0 & 0 \\ 0 & -1 & 0 & -1 & 0 & 6 & 0 & -4 & 0 & 0 & 0 & 0 \\ 0 & 0 & 0 & 0 & -4 & 0 & 32 & 0 & 16 & 0 & 16 & 0 \\ 0 & 0 & 0 & 0 & 0 & -4 & 0 & 32 & 0 & 16 & 0 & 16 \\ -4 & 0 & 0 & 0 & 0 & 0 & 16 & 0 & 32 & 0 & 16 & 0 \\ 0 & -4 & 0 & 0 & 0 & 0 & 0 & 16 & 0 & 32 & 0 & 16 \\ 0 & 0 & -4 & 0 & 0 & 0 & 16 & 0 & 16 & 0 & 32 & 0 \\ 0 & 0 & 0 & -4 & 0 & 0 & 0 & 16 & 0 & 16 & 0 & 32 \end{bmatrix} \tag{70}$$

Using the transformation (65), a possible mass matrix for the LST-6/12R configuration is

$$\mathbf{M}_L = \mathbf{T}_{CR}^T \mathbf{M}_C \mathbf{T}_{CR}, \tag{71}$$

which is easily obtained in closed form. This mass matrix has a rank deficiency of one if $\alpha \neq 0$, with the null eigenvector (66). However rank deficiency of mass matrices is not that important as in stiffness matrices, unless they are used in explicit transient analysis.

The mass matrix $\mathbf{M}_L$ depends on the parameter α present in $\mathbf{T}_{RC}$. To find the best value α_M when this mass is paired to the OPT stiffness it is convenient to morph the mass into that of a

Bernoulli-Euler beam following the technique outlined in Section 5.5: $\mathbf{M}_{beam} = \mathbf{T}_m^T \mathbf{M}_L \mathbf{T}_m$. Then the plane-wave Fourier analysis described in [42,43] on a repeating beam lattice is carried out. The end result for the computed nondimensional acoustic frequency is the dispersion relation

$$\omega_a^2 = k^4 + \frac{1 + (17 + 2\alpha)\gamma^2 + (16\alpha - 23)\gamma^4 + (2\alpha - 3)\gamma^6}{12\gamma^2(1 + 8\gamma^2 + \gamma^4)} k^6 + O(k^8) \tag{72}$$

where k is the wavenumber. The exact nondimensional acoustic frequency is $\omega_a^2 = k^4$. Because of the dependence on γ, the term in k^6 cannot be made to vanish for a specific α. But it rapidly tends to zero for $\gamma >> 1$ if $\alpha_M = \alpha = 3/2$, which is the recommended value. (Note that this differs from the recommended value for the retrofitted stiffness, which is $\alpha_b = 4/3$. But the mass-stiffness pairing of $\mathbf{M}_L$ is not with $\mathbf{K}_L$, but with that of the optimal element.)

8. THE ALLMAN 1988 TRIANGLE

In 1984 Allman published [47] a drilling freedom triangle based on quadratic shape functions. This element is a clone of that presented in Section 7 if one takes $\alpha_b = 1$. It is therefore rank deficient. This was corrected in a subsequent publication [48].

8.1. Shape Functions

The displacement interpolation used in the 1988 element is

$$\begin{aligned} u_x &= N_{xx1} u_{x1} + N_{xy1} u_{y1} + N_{x\theta 1}\theta_1 + \ldots + N_{x\theta 3}\theta_3, \\ u_y &= N_{yx1} u_{x1} + N_{yy1} u_{y1} + N_{y\theta 1}\theta_1 + \ldots + N_{y\theta 3}\theta_3. \end{aligned} \tag{73}$$

where the shape functions are

$$\begin{aligned} &N_{xx1} = \zeta_1 - x_{23}x_{r0},\ N_{xy1} = -y_{23}x_{r0},\ N_{xx2} = \zeta_2 - x_{31}x_{r0},\ N_{xy2} = -y_{31}x_{r0}, \\ &N_{xx3} = \zeta_3 - x_{12}x_{r0},\ N_{xy3} = -y_{12}x_{r0},\ N_{x\theta 1} = \tfrac{1}{2}(-g_1\zeta_{12} + g_5\zeta_{31} + g_1\zeta_{1221} + g_5\zeta_{3113}), \\ &N_{x\theta 2} = \tfrac{1}{2}(-g_3\zeta_{23} + g_1\zeta_{12} + g_3\zeta_{2332} + g_1\zeta_{1221}),\ N_{x\theta 3} = \tfrac{1}{2}(-g_5\zeta_{31} + g_3\zeta_{23} + g_5\zeta_{3113} + g_3\zeta_{2332}), \\ &N_{yx1} = -x_{23}y_{r0},\ N_{yy1} = \zeta_1 - y_{23}y_{r0},\ N_{yx2} = -x_{31}y_{r0},\ N_{yy2} = \zeta_2 - y_{31}y_{r0}, \\ &N_{yx3} = -x_{12}y_{r0},\ N_{yy3} = \zeta_3 - y_{12}y_{r0},\ N_{y\theta 1} = \tfrac{1}{2}(-g_2\zeta_{12} + g_6\zeta_{31} + g_2\zeta_{1221} + g_6\zeta_{3113}), \\ &N_{y\theta 2} = \tfrac{1}{2}(-g_4\zeta_{23} + g_2\zeta_{12} + g_4\zeta_{2332} + g_2\zeta_{1221}),\ N_{y\theta 3} = \tfrac{1}{2}(-g_6\zeta_{31} + g_4\zeta_{23} + g_6\zeta_{3113} + g_4\zeta_{2332}). \end{aligned} \tag{74}$$

in which

$$\begin{aligned} &\zeta_{12} = \zeta_1\zeta_2,\ \zeta_{23} = \zeta_2\zeta_3,\ \zeta_{31} = \zeta_3\zeta_1,\ \zeta_{1221} = \zeta_{12}(\zeta_2 - \zeta_1),\ \zeta_{2332} = \zeta_{23}(\zeta_3 - \zeta_2), \\ &\zeta_{3113} = \zeta_{31}(\zeta_1 - \zeta_3),\ a_{12} = 2A/L_{12},\ b_{12} = (x_{12}x_{13} + y_{12}y_{13})/L_{12},\ a_{23} = 2A/L_{23}, \\ &b_{23} = (x_{23}x_{21} + y_{23}y_{21})/L_{23},\ a_{31} = 2A/L_{31},\ b_{31} = (x_{31}x_{32} + y_{31}y_{32})/L_{31}, \\ &x_{p12} = x_{21}b_{12}/L_{12} + x_1,\ y_{p12} = y_{21}b_{12}/L_{12} + y_1,\ x_{p23} = x_{32}b_{23}/L_{23} + x_2, \\ &y_{p23} = y_{32}b_{23}/L_{23} + y_2,\ x_{p31} = x_{13}b_{31}/L_{31} + x_3,\ y_{p31} = y_{13}b_{31}/L_{31} + y_3, \\ &g_1 = L_{12}(x_{p12} - x_3)/a_{12},\ g_2 = L_{12}(y_{p12} - y_3)/a_{12},\ g_3 = L_{23}(x_{p23} - x_1)/a_{23}, \\ &g_4 = L_{23}(y_{p23} - y_1)/a_{23},\ g_5 = L_{31}(x_{p31} - x_2)/a_{31},\ g_6 = L_{31}(y_{p31} - y_2)/a_{31}, \\ &x_{r0} = (g_1\zeta_{1221} + g_3\zeta_{2332} + g_5\zeta_{3113})/(4A),\ y_{r0} = (g_2\zeta_{1221} + g_4\zeta_{2332} + g_6\zeta_{3113})/(4A), \end{aligned} \tag{75}$$

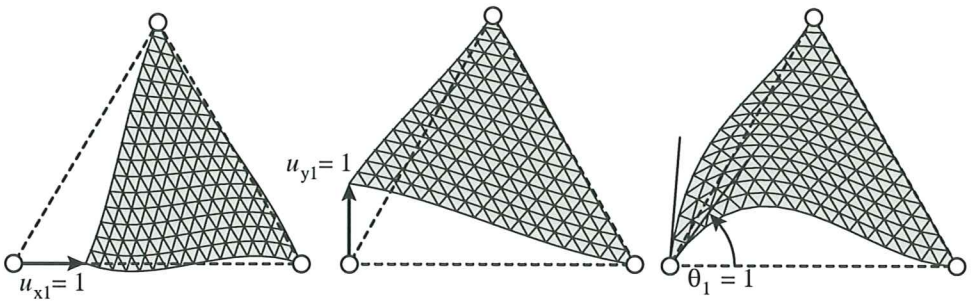

Figure 14. Shape functions for corner 1 of Allman 1988 triangle.

The shape functions for the three freedoms of corner node 1 are plotted in Figure 14. In contrast to those of Figure 13, all shape functions are nonconforming. The strain-displacement matrix $\mathbf{e} = \mathbf{Bu}$ is readily computed by differentiation of the shape functions. The stiffness matrix is then obtained as

$$\mathbf{K}_A = \int_{\Omega^e} h\, \mathbf{B}^T\, \mathbf{E}\, \mathbf{B}\, d\Omega, \tag{76}$$

where $d\Omega$ is the element of area. Variants of this element result according to the integration rule adopted in (76). These are studied next.

8.2. Variants

Since the shape functions (73) are cubic, the derived strains vary quadratically. For uniform $\mathbf{E}$ and h the integrand of (76) varies quartically. Exact integration may be achieved with the 7-point Gauss rule for triangles. For an isotropic material the exactly integrated element, has the bending energy ratio listed in Table 3 under label ALL-EX. This has γ^4 growth and hence rapidly locks for high aspect ratios.

As the optimal element of Section 5 has linearly varying strains, it is of interest to see whether filtering the strains to a linear variation improves the bending behavior. One way of linearizing strains is by reducing the integration rule. Consider the 3-point triangle quadrature rule defined parametrically by

$$\int_A F(\zeta_1, \zeta_2, \zeta_3)\, dA \approx \frac{A}{3}\Big[F\,(\xi, \xi, 1-2\xi) + F\,(\xi, 1-2\xi, \xi) + F\,(1-2\xi, \xi, \xi)\Big] \tag{77}$$

where $0 \le \xi \le \frac{1}{2}$. The two useful rules of this type are $\xi = 1/6$ (the interior-three-point rule) and $\xi = 1/2$ (the midpoint rule), both of which exhibit quadratic accuracy. But in the present context it is instructive to leave initially ξ free. A symbolic analysis with *Mathematica* shows that if the 1988 Allman element is numerically integrated by (77), the stiffness matrix is an instance of template (31) with

$$\begin{aligned} &\alpha_b = 4\xi(2-3\xi), \quad \beta_0 = \tfrac{4}{9}, \quad \beta_1 = \tfrac{1}{2}\xi, \quad \beta_2 = \tfrac{5}{2}\xi, \quad \beta_3 = 3\xi, \\ &\beta_4 = 0, \quad \beta_5 = 2\xi, \quad \beta_6 = -2\xi, \beta_7 = -\tfrac{1}{2}\xi, \quad \beta_8 = -3\xi, \quad \beta_9 = -\tfrac{5}{2}\xi. \end{aligned} \tag{78}$$

Inserting into (36)–(38) the bending energy ratio r is readily obtained. Results for particular cases $\xi = 1/2$ and $\xi = 1/6$ are listed in Table 3 under labels ALL-3M and ALL-3I, respectively.

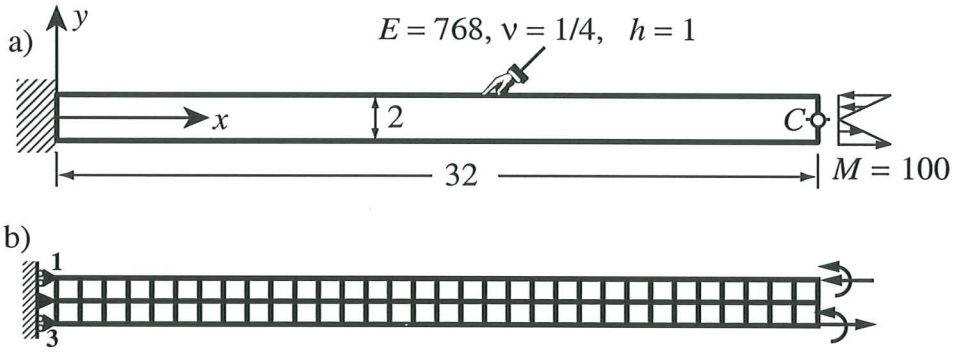

Figure 15. Slender cantilever beam under end moment: root contraction allowed; four-overlaid-triangle mesh units; a 32 × 2 mesh is shown in (b).

Yet another way to fit a linear strain pattern to Allman's quadratic strain fit is by minimizing a dislocation potential, which results in a least-square-like fit. The resulting element is called ALL-LS. One finds that this element is an instance of the template (31) with the parameters shown in Table 2. The energy ratio is given in Table 3.

It can be seen that all variants of the Allman element exhibit catastrophic aspect ratio locking with r growing as γ^4 for $\gamma >> 1$. Of the four variants shown in Tables 1–3, ALL-3I is preferable since it has the lowest r as γ grows. But all of them are worse than the humble CST when $\gamma > 8$.

9. NUMERICAL EXAMPLES

References [19,23] contain extensive comparisons of triangular elements with drilling freedoms, as does the thesis of Nygård [25] for both triangles and quadrilaterals. Only three numerical examples are presented here. The first two are standard benchmarks that focus on the effect of aspect ratio on the bending response. The third (Cook's problem) is included since there are published results for many element types.

9.1. Example 1: Cantilever under End Moment

The slender cantilever beam of Figure 15 is subjected to an end moment $M = 100$. The modulus of elasticity is set to $E = 768$ so that the exact tip deflection $\delta_{tip} = ML/(2EI)$ is 100. Regular meshes ranging from 32 × 2 to 2 × 2 are used, each rectangle mesh unit being composed of four half-thickness overlaid triangles. The element aspect ratios vary from 1:1 through 16:1. The root clamping condition is imposed by setting

$$u_{x1} = u_{x2} = u_{x3} = 0, \quad u_{y2} = 0, \quad \theta_{x1} = \theta_{x2} = \theta_{x3} = 0, \tag{79}$$

where 1, 2, 3 are the root nodes, numbered from the top. It is important to leave u_{y1} and u_{y3} unrestrained for $\nu \neq 0$. This allows for the Poisson's contraction at the root and makes the exact solution merge with the displacement solution given in Section 5.1 over the entire beam.

Table 4 reports computed tip deflections (y displacement at C). for several element types and five aspect ratios. The identifiers in the "load lumping" column define ways in which the applied tractions at the free end are transformed to node forces; this topic is elaborated upon in [20].

Table 4 Tip Deflections (exact=100) for Cantilever under End Moment

Element	Load Lumping	Mesh: x-subdivisions × y-subdivisions				
		32 × 2 ($\gamma = 1$)	16 × 2 ($\gamma = 2$)	8 × 2 ($\gamma = 4$)	4 × 2 ($\gamma = 8$)	2 × 2 ($\gamma = 16$)
ALL-3I	EBQ	87.08	76.48	38.32	5.42	0.39
ALL-3M	EBQ	81.36	53.57	9.59	0.71	0.04
ALL-EX	EBQ	84.90	69.09	24.23	2.47	0.16
ALL-LS	EBQ	85.36	68.25	20.83	1.89	0.12
CST	LI	54.05	36.36	15.75	4.82	1.28
FF84	EBQ	98.36	97.17	96.58	96.34	96.27
LST-Ret	EBQ	89.05	81.04	59.58	28.93	9.46
OPT	EBQ	99.99	99.99	99.99	99.96	100.07

Because two elements through the height are used, the computed deflections should be $100/r^{(2)}$, where $r^{(2)} = (3 + r)/4$ as per equation (42). This provides a valuable numerical confirmation of the energy ratios listed in Table 3. Discrepancies from that prediction are due to load lumping schemes. For example, the results for OPT should be exactly 100.00 for any γ. And in fact they are if another load lumping scheme labeled EBZ in [20] is used. But the effect of the load lumping is slight, affecting only the fourth place of the computed deflections. The tiny deviations from 100.00 are due to scheme EBQ not being in exact energy balance, as explained in that reference.

The FF84 element maintains good but not perfect accuracy. The Allman 88 triangles perform well for unit aspect ratios but rapidly become overstiff for $\gamma > 2$; all variants are inferior to the CST for $\gamma > 9$. Of the four variants listed in Table 4 ALL-3I is consistently superior.

9.2. Example 2: The Shear-Loaded Berkeley Cantilever

The shear-loaded cantilever beam defined in Figure 16 has been selected as a test problem for plane stress elements by many investigators since originally proposed in [12]. A full root-clamping condition is implemented by constraining both displacement components to zero at nodes located on at the root section $x = 0$. Drilling rotations must not be constrained at the root because the term $\partial u_y/\partial x$ in the continuum-mechanics definition is nonzero there. The applied shear load varies parabolically over the end section and is consistently lumped at the nodes.

The main comparison value is the tip deflection $\delta_C = u_{yC}$ at the center of the end-loaded cross section. One perplexing question concerns the analytical value of δ_C. An approximate solution derived from 2-D elasticity (based on a polynomial Airy stress function) gives $\delta_{el} = 0.34133 + 0.01400 = 0.35533$, where the first term comes from the bending deflection $PL^3/3EI_{zz}$, $I_{zz} = hH^3/12$, and the second from a y-quadratic shear field. The shear term coefficient in the second term results from assuming a warping-allowed root-clamping condition that is more "relaxed" than the fully-clamped condition prescribed on the FE model. Consequently in [12] it was argued that δ_{el} should be an upper bound, which was verified by the conforming FE models tested at that time. The finest grid results in [23] gave, however, $\delta_C \approx 0.35587$, which exceeds that "bound" in the fourth place. The finest OPT mesh ran here (128 × 32) gave a still larger value: 0.35601. The apparent explanation for this paradox is that if $\nu \neq 0$, a mild singularity in σ_{yy} and τ_{xy}, induced by the restraint $u_y|_{x=0} = 0$, develops at the corners of the root section, as depicted in Figure 17. This singularity "clouds" convergence of digits 4-5. (In retrospect it would have been better to allow for lateral contraction effects as in Example 1 to avoid this singularity.) The percentage results in

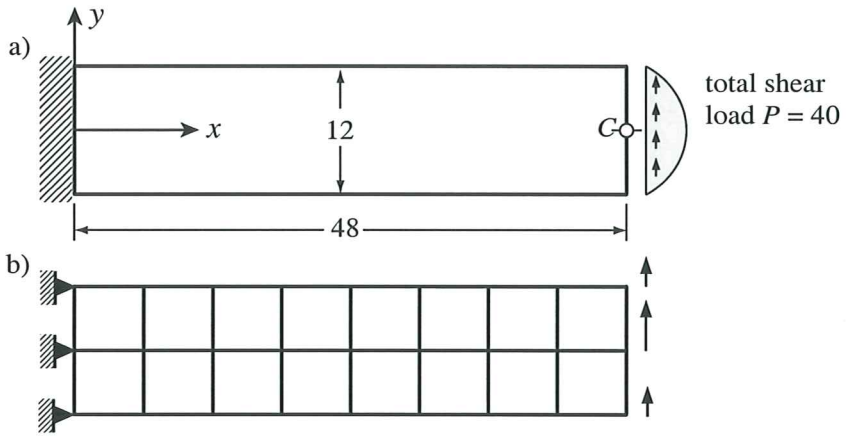

Figure 16. Cantilever under end shear: $E = 30000$, $\nu = 1/4$, $h = 1$; root contraction not allowed; four-overlaid-triangle mesh units; a 8×2 mesh is shown in (b).

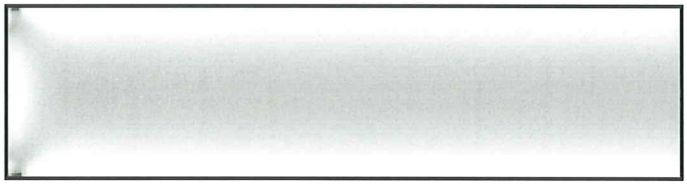

Figure 17. Intensity contour plot of σ_{xy} given by the 64×16 OPT mesh. Stress node values averaged between adjacent elements. The root singularity pattern is visible.

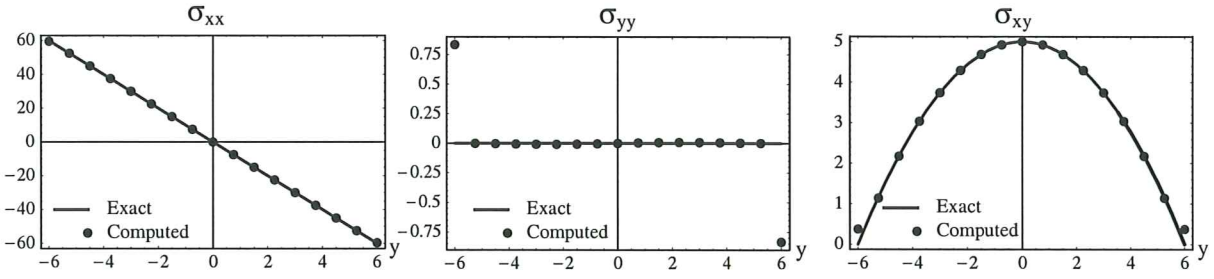

Figure 18. Distributions of σ_{xx}, σ_{yy} and σ_{xy} at $x = 12$ given by the 16×64 OPT mesh. Stress node values averaged between adjacent elements. Note different stress scales. Deviations at $y = \pm 6$ (free edges) due to "upwinded" y averaging.

Tables 3-5 of [23] therefore contain errors in the 4th place.

Table 5 gives computed deflections for rectangular mesh units with aspect ratios of 1, 2 and 4. Mesh units consist of four half-thickness overlaid triangles. For reporting purposes the load was scaled by 100/0.35601 so that the "theoretical solution" becomes 100.00.

The data in Table 5 generally follows the patterns of the previous example; the main difference being the lack of drastically small deflections because element aspect ratios only go up to 4:1. Of

Table 5 Tip Deflections (exact = 100) for Short Cantilever under End Shear

Element	Mesh: x-subdivisions × y-subdivisions				
	8 × 2	16 × 4	32 × 8	64 × 16	128 × 32
ALL-3I	96.41	98.59	99.59	99.91	99.99
ALL-3M	82.70	94.78	98.57	99.62	99.91
ALL-EX	89.43	96.88	99.16	99.79	99.96
ALL-LS	89.72	96.94	99.17	99.79	99.96
CST	55.09	82.59	94.90	98.65	99.66
FF84	99.15	99.71	99.87	99.96	99.99
LST-Ret†	70.86	91.10	97.90	99.56	99.90
OPT	101.68	100.30	100.03	100.00	100.00
	4 × 2	8 × 4	16 × 8	32 × 16	64 × 32
ALL-3I	82.27	93.22	97.86	99.38	99.83
ALL-3M	54.23	81.84	94.52	98.50	99.61
ALL-EX	70.71	89.63	96.93	99.15	99.77
ALL-LS	69.97	89.30	96.94	99.17	99.79
CST	37.85	69.86	90.04	97.25	99.28
FF84	94.27	97.85	99.23	99.74	99.92
LST-Ret†	79.58	93.53	98.14	99.49	99.83
OPT	96.68	98.44	99.37	99.78	99.93
	2 × 2	4 × 4	8 × 8	16 × 16	32 × 32
ALL-3I	42.53	72.66	90.72	97.32	99.27
ALL-3M	12.39	31.81	63.68	87.24	96.41
ALL-EX	26.16	56.93	83.54	95.14	98.69
ALL-LS	23.02	52.37	80.84	94.22	98.45
CST	17.83	43.84	75.01	92.13	97.86
FF84	89.26	96.37	98.66	99.50	99.83
LST-Ret†	56.71	83.79	95.14	98.63	99.62
OPT	92.24	96.99	98.70	99.48	99.81

† Requires one drilling freedom to be fixed, else stiffness is singular.

the four Allman triangle versions again ALL-3I outperformed the others. The results for FF84 and OPT triangles are very similar, without the latter displaying the clear advantages of Example 1. The data for FF84 and CST changes slightly from that of Tables 3-5 of [23] on two accounts: four-triangle, rather than two-triangle, macroelements are used to eliminate y-directionality, and the normalizing "theoretical" solution changes by +0.00014 as explained above.

Figure 18 plots averaged node stress values at section $x = 12$ computed from the 64 × 16 OPT mesh. The recovery is based on (46) with $\beta_0^e = 3/2$. The agreement with the standard beam stress distribution (the section is sufficiently away from the root) is very good at interior points but less so at the free edges $y = \pm 6$ since the averaging becomes biased.

9.3. Example 3: Cook's Problem

Table 6 gives results computed for the plane stress problem defined in Figure 19. This problem was proposed by Cook [49] as a test case for nonrectangular quadrilateral elements. There is no known analytical solution but the OPT results for the 64 × 64 mesh may be used for comparison purposes. (Extrapolation of the OPT results using Wynn's ϵ algorithm [50] yields $u_{yC} = 23.956$.)

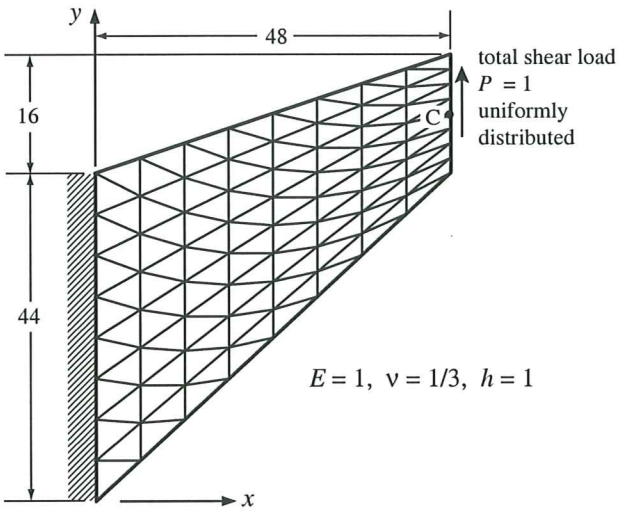

Figure 19. Cook's problem: clamped trapezoid under end shear. A 8 × 8 mesh is shown.

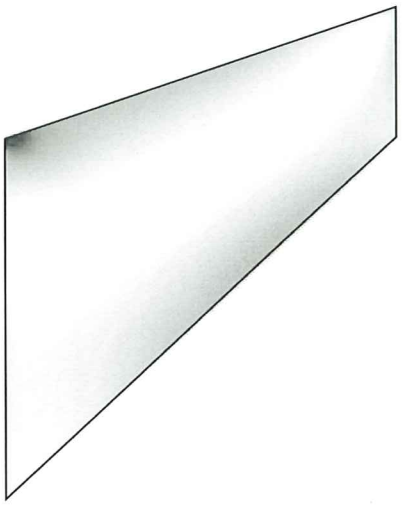

Figure 20. von Mises stress intensity distribution from 32 × 32 OPT element mesh. Peak occurs at upper left corner.

The last six lines in Table 6 pertain to quadrilateral elements. Results for HL, HG and Q4 are taken from [49] whereas those for Q6 and QM6 are taken from [51]. Results for the Free Formulation quadrilateral FFQ are taken from Nygård's thesis [25]. Further data on other elements is provided in [52].

For triangle tests, quadrilaterals were assembled with two triangles in the shortest-diagonal-cut layout as illustrated in Figure 16 for a 2 × 2 mesh. Cutting the quadrilaterals the other way or using four-overlaid-triangle macroelements yields stiffer results.

Since element aspect ratios are reasonable near the root (where the action is), the performance of the seven LST-3/9R models tested can be expected to be similar, and indeed it was. Of the seven

Table 6 Results for Cook's Problem

	Vertical deflection at C for subdivision					
Element	2 × 2	4 × 4	8 × 8	16 × 16	32 × 32	64 × 64
ALL-3I	21.61	23.00	23.66	23.88	23.94	
ALL-3M	16.61	21.05	23.02	23.69	23.87	
ALL-EX	19.01	21.83	23.43	23.81	23.91	
ALL-LS	19.43	22.32	23.44	23.82	23.92	
CST	11.99	18.28	22.02	23.41		
FF84	20.36	22.42	23.41	23.79	23.91	
LST-Ret†	19.82	22.62	23.58	23.86	23.94	
OPT	20.56	22.45	23.43	23.80	23.91	23.95
FFQ	21.66	23.11	23.79	23.88	23.94	
HL	18.17	22.03		23.81		
HG	22.32	23.23		23.91		
Q4	11.85	18.30		23.43		
Q6	22.94	23.48				
QM6	21.05	23.02				

† Requires one drilling DOF to be fixed, else stiffness is singular

ALL-3I is best followed closely by LST-Ret, OPT and FF84. It should be noted that accuracy of the FF84 and OPT triangles for this problem is dominated by the basic stiffness response. Consequently the deflection values provided by the FF84 and OPT elements, which share the same basic stiffness, are very close.

The overall stress distribution for this problem is rarely reported. Figure 18 displays a *Mathematica*-generated intensity contour plot of the von Mises stress computed from the 32 × 32 OPT mesh, using the recovery formula (46) with $\beta_0^e = 3/2$. A singularity pattern at point $\{x = 0, y = 44\}$, which is located at a fixed entrant corner, is evident.

10. DISCUSSION AND CONCLUSIONS

The conclusions are posted below in a Q&A format so that readers can scan subjects quickly.

Has the OPT triangle been used much?

The optimal LST-3/9R element has been used since 1991 as membrane component of a shell element with 6 DOF per corner. The presence of the drilling freedom facilitates modeling of surface intersections and stiffeners. In fact the shell element is so fast and versatile that it has largely replaced beams in modeling complete aircraft structures. Figure 21 shows portion of the interior structure of an F-16 used in aeroelastic studies by Farthat's team [53]: note that triangles are used for any thin wall component. A corotational version developed by Haugen [54] is used in the FEDEM multibody dynamics system. The FF84 ancestor is used in Norwegian codes developed at Trondheim by Pål Bergan and colleagues.

When is exact pure-bending response important?

Bending response exactness for any aspect ratio γ is important in modeling thin and composite aerospace structures, such as the stiffened panel depicted in Figure 22. If the longitudinal direction

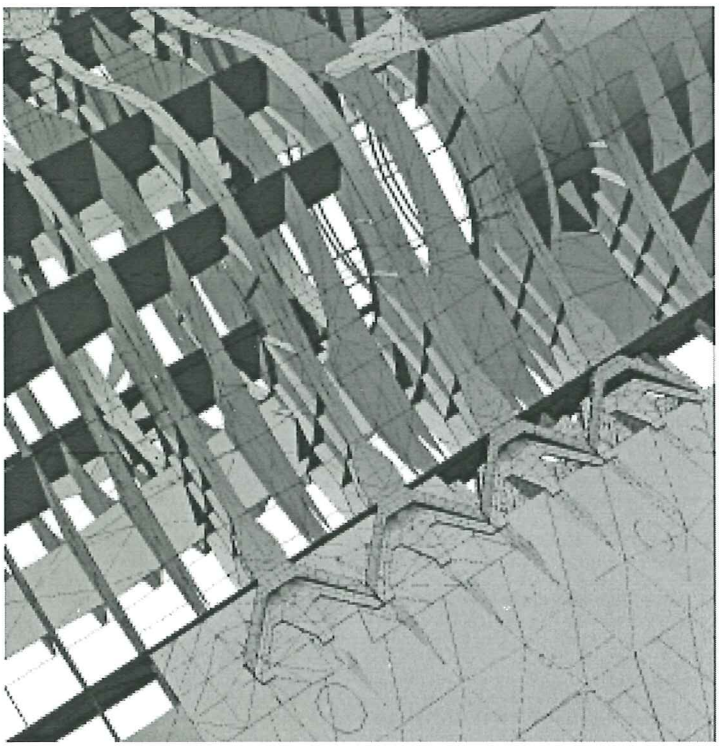

Figure 21. Internal structure of an F16 fighter modeled with triangle shell elements (courtesy Greg Brown).

called x in the bending test is set along the panel, that Figure shows a very high γ in a flange and a small γ in a joint. Aspect ratio locking in such mesh units can adversely affect the response of the whole structure.

What are the major advantages of templates?

The obvious one is the possibility of searching for optimal or custom element instances, without worry as to fixing up bad elements along the way. They are also useful in research studies because a template spans an infinity of possible elements including elements already published. This unification facilitates comparison of previous and new elements using a single implementation, as in Figure 10.

Why are strains good choice for higher order trial spaces?

Strains are intermediate variables between displacements and stresses. Unlike them, no boundary conditions can be applied on strains. This mediatory nature tends to produce elements of balanced behavior: neither too stiff nor too flexible. In non-mechanical problems, the same role can be assigned to the intermediate variable that appears in Tonti diagrams of the variational formulation [38].

Do templates supersede conventional element derivation methods?

No. The template configuration, by which it is meant the sequence of matrix products and the functional dependence of matrix entries on geometry and constitutive properties, has to be established by conventional methods. For example, the ANDES formulation leads to the forms (28)–(31),

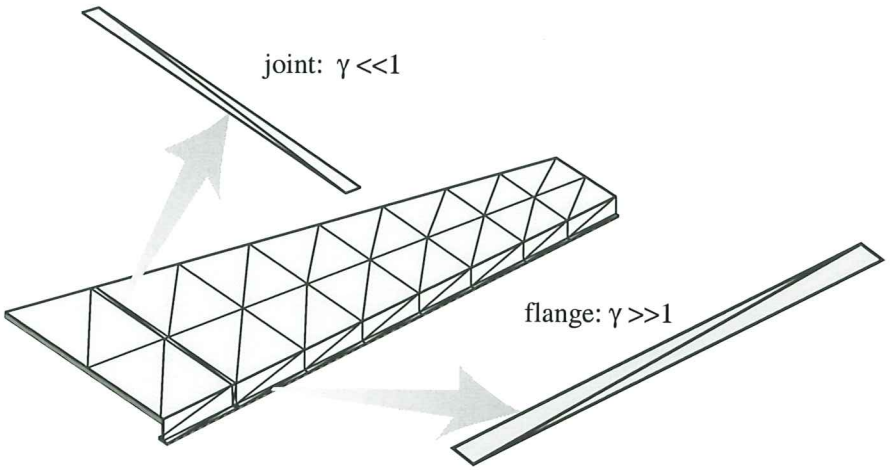

Figure 22. Stiffened panels modeled by facet shell elements are a common source of high aspect ratio elements.

which could not be guessed *a priori*. Parameters are injected as weights of algebraic terms as appropriate.

I have derived an alledgely new LST-3/9R triangle. How do I check if it is optimal?

The first step is to run the bending ratio test of Section 5.1, numerically or (better) symbolically. If: (i) the ratio $r = 1$ for all γ, (ii) the element passes the ordinary patch tests and (iii) is rank sufficient, it is indeed optimal. But is it new? The next step should be to try the test geometry of Section 6 and compare $\mathbf{K}$ to (49). If it matches, the "new triangle" is likely a clone of the OPT element. This can be rigurously proven by extracting its template signature, which is not a easy process if the element was fabricated as a whole. If it does not match you have a different optimal element. As discussed in Section 5.4, this cannot happen if the element is energy orthogonal.

Should parameters be left as arguments of element implementations?

Only for research studies, and to find clones (as in the scenario of the foregoing question). In production implementations parameters should be hardwired to a name, as illustrated by the module listed in Figure 12. Few users have the knowledge or interest to play around with parameter values.

Why is it worth republishing the optimal element?

Two reasons. First, the fact that a membrane element with this freedom configuration that is insensitive to aspect ratio can be constructed does not seem to be generally known. Second, the derivation can be now comfortably placed within the framework of finite element templates, which was an embryonic concept ten years ago. As a result, several elements in common use can be exhibited as instances of the ANDES template, facilitating unified implementation and testing.

The paper discusses three models, but more have been published. Why the omission?

The three models are intended to illustrate the derivation approaches of Figure 1. The ANDES template exemplifies the direct fabrication approach. The retrofitted LST is a textbook example of, well, the retrofitting approach. The Allman 1984 triangle displays the typical tribulations of the fixed-up approach in that several variants are tried but none cures aspect ratio locking. Including more models would have lenghtened the exposition without achieving appreciable benefits over the optimal one.

Appendix A. THE HIGHER ORDER STRAIN FIELD

For completeness the construction of the higher order strain field carried out in Ref [19] is summarized here. Split the hierarchical rotations into mean and deviatoric: $\tilde{\theta}_1 = \bar{\theta} + \theta'_1$, $\theta_2 = \bar{\theta} + \theta'_2$, $\theta_3 = \bar{\theta} + \theta'_3$, where $\bar{\theta} = \frac{1}{3}(\tilde{\theta}_1 + \tilde{\theta}_2 + \tilde{\theta}_3)$. In matrix form: $\tilde{\boldsymbol{\theta}} = \bar{\boldsymbol{\theta}} + \boldsymbol{\theta}'$ where $\bar{\boldsymbol{\theta}} = \bar{\theta}\,[\,1\ 1\ 1\,]^T$ and $\boldsymbol{\theta}' = [\,\theta'_1\ \theta'_2\ \theta'_3\,]^T$. The deviatoric corner rotations define the linear deviatoric-rotation field:

$$\theta' = \theta'_1\zeta_1 + \theta'_2\zeta_2 + \theta'_3\zeta_3, \tag{80}$$

which integrates to zero over the element. For subsequent use we note the matrix relation

$$\begin{bmatrix} \theta'_1 \\ \theta'_2 \\ \theta'_3 \\ \bar{\theta} \end{bmatrix} = \left(\begin{bmatrix} 1 & 0 & 0 \\ 0 & 1 & 0 \\ 0 & 0 & 1 \\ \frac{1}{3} & \frac{1}{3} & \frac{1}{3} \end{bmatrix} - \frac{1}{3}\begin{bmatrix} 1 & 1 & 1 \\ 1 & 1 & 1 \\ 1 & 1 & 1 \\ 0 & 0 & 0 \end{bmatrix} \right) \begin{bmatrix} \tilde{\theta}_1 \\ \tilde{\theta}_2 \\ \tilde{\theta}_3 \end{bmatrix} = \frac{1}{3}\begin{bmatrix} 2 & -1 & -1 \\ -1 & 2 & -1 \\ -1 & -1 & 2 \\ 1 & 1 & 1 \end{bmatrix} \begin{bmatrix} \tilde{\theta}_1 \\ \tilde{\theta}_2 \\ \tilde{\theta}_3 \end{bmatrix}. \tag{81}$$

The splitting (81) translates to a similar decomposition of the higher order strains: $\mathbf{e}_d = \mathbf{e}_b + \mathbf{e}_t$. where subscripts b and t identify "pure bending" and "torsional" strain fields, respectively. These are generated by the deviatoric rotations $\boldsymbol{\theta}'$ and the mean hierarchical rotation $\bar{\theta}$, respectively.

A.1 The Pure Bending Field

This field is produced by the deviatoric corner rotations θ'_i, $i = 1, 2, 3$, inducing the side-aligned natural strains

$$\boldsymbol{\epsilon}_b = [\,\epsilon_{b21}\quad \epsilon_{b32}\quad \epsilon_{b13}\,]^T. \tag{82}$$

pertaining to choise (s) in Figure 5. The *straingage locations* are chosen at the triangle corners. The natural strain ϵ_{jk} at corner i is written $\epsilon_{jk|i}$, the bar being used for reading convenience. Vector $\boldsymbol{\epsilon}_b$ at corner i is denoted by $\boldsymbol{\epsilon}_{bi}$. The goal is to construct the 3×3 matrices $\mathbf{Q}_{bi}$ that relate natural straingage readings to the deviatoric rotations:

$$\boldsymbol{\epsilon}_{b1} = \mathbf{Q}_{b1}\boldsymbol{\theta}', \qquad \boldsymbol{\epsilon}_{b2} = \mathbf{Q}_{b2}\boldsymbol{\theta}', \qquad \boldsymbol{\epsilon}_{b3} = \mathbf{Q}_{b3}\boldsymbol{\theta}', \tag{83}$$

Once these are known the natural bending strains can be obtained by linear interpolation over the triangle: $\boldsymbol{\epsilon}_b = (\mathbf{Q}_{b1}\zeta 1 + \mathbf{Q}_{b2}\zeta_2 + \mathbf{Q}_{b3}\zeta_3)\boldsymbol{\theta}' = \mathbf{Q}_b\,\boldsymbol{\theta}'$. Consider $\epsilon_{b21}(P)$ at an arbitrary point P of the triangle. Denote by $d_{21|P}$ the signed distance from the centroid to P measured along the internal normal to side 21, and specialize P to corners:

$$d_{21|3} = \frac{4A}{3\ell_{21}}, \qquad d_{21|1} = d_{21|2} = -\tfrac{1}{2}d_{21|3} = -\frac{2A}{3\ell_{12}}. \tag{84}$$

Assume that $\epsilon_{b21|P}$ depends only on $d_{21|P}$ divided by the side length ℓ_{21}, which introduces a distance scaling. These dimensionless ratios will be called $\chi_{21|P} = d_{21|P}/\ell_{21}$, which specialized to the corners become

$$\chi_{21|3} = \frac{4A}{3\ell_{21}^2}, \qquad \chi_{21|1} = \chi_{21|2} = -\frac{2A}{3\ell_{21}^2}. \tag{85}$$

Formulas for corners 2 and 3 are obtained by cyclic permutation. According to the foregoing assumption, the natural straingage readings $\epsilon_{b21|i}$ at corner i depend only on $\chi_{21|i}$, multiplied by as yet unknown weighting factors. In matrix form:

$$\boldsymbol{\epsilon}_{b1} = \begin{bmatrix} \epsilon_{b21|1} \\ \epsilon_{b32|1} \\ \epsilon_{b13|1} \end{bmatrix} = \frac{2A}{3}\begin{bmatrix} \frac{\psi_1}{\ell_{21}^2} & \frac{\psi_2}{\ell_{21}^2} & \frac{\psi_3}{\ell_{21}^2} \\ \frac{\psi_4}{\ell_{32}^2} & \frac{\psi_5}{\ell_{32}^2} & \frac{\psi_6}{\ell_{32}^2} \\ \frac{\psi_7}{\ell_{13}^2} & \frac{\psi_8}{\ell_{13}^2} & \frac{\psi_9}{\ell_{13}^2} \end{bmatrix} \begin{bmatrix} \theta'_1 \\ \theta'_2 \\ \theta'_3 \end{bmatrix} = \mathbf{Q}_{b1}\boldsymbol{\theta}'. \tag{86}$$

Here ψ_1 through ψ_9 are dimensionless weight parameters. (In [19] five parameters called ρ_1 through ρ_5 are used instead, cf. equation (19); these account *a priori* for triangular symmetries as noted in Section 4.6.) Relations for corners 2 and 3 are constructed by cyclic permutation.

Pictures of the unweighted bending modes are shown in Figure 7. These were obtained by integrating the strain field into displacements, which is possible since both natural and Cartesian strains vary linearly.

A.2 The Torsional Field

The higher order stiffness produced by the pure bending field alone is rank deficient by one because of the deviatoric constraint $\theta_1' + \theta_2' + \theta_3' = 0$. To get rank sufficiency it is necessary to build a strain field associated with $\tilde{\theta}_i = \bar{\theta}$, others zero. This may be viewed as forcing each corner of the triangle to rotate by the same amount while the corner displacements are precluded. A displacement-based solution to this problem is provided by the cubic field of the QST4-20G shown in the center of Figure 2. From [12, p. 30] the shape function interpolation for u_x is

$$u_x(\zeta_1, \zeta_2, \zeta_3) = \begin{bmatrix} u_{x1} \\ u_{x,x\vert1} \\ u_{x,y\vert1} \\ u_{x2} \\ u_{x,x\vert2} \\ u_{x,y\vert2} \\ u_{x3} \\ u_{x,x\vert3} \\ u_{x,y\vert3} \\ u_{x0} \end{bmatrix}^T \begin{bmatrix} \zeta_1^2(3-2\zeta_1) - 7\zeta_1\zeta_2\zeta_3 \\ \zeta_1^2(x_{21}\zeta_2 - x_{13}\zeta_3) + (x_{13} - x_{21})\zeta_1\zeta_2\zeta_3 \\ \zeta_1^2(y_{21}\zeta_2 - y_{13}\zeta_3) + (y_{13} - y_{21})\zeta_1\zeta_2\zeta_3 \\ \zeta_2^2(3-2\zeta_2) - 7\zeta_1\zeta_2\zeta_3 \\ \zeta_2^2(x_{32}\zeta_3 - x_{21}\zeta_1) + (x_{21} - x_{32})\zeta_1\zeta_2\zeta_3 \\ \zeta_2^2(y_{32}\zeta_3 - y_{21}\zeta_1) + (y_{21} - y_{32})\zeta_1\zeta_2\zeta_3 \\ \zeta_3^2(3-2\zeta_3) - 7\zeta_1\zeta_2\zeta_3 \\ \zeta_3^2(x_{13}\zeta_1 - x_{32}\zeta_2) + (x_{32} - x_{13})\zeta_1\zeta_2\zeta_3 \\ \zeta_3^2(y_{13}\zeta_1 - y_{32}\zeta_2) + (y_{32} - y_{13})\zeta_1\zeta_2\zeta_3 \\ 27\zeta_1\zeta_2\zeta_3 \end{bmatrix} \tag{87}$$

where $u_{x,x\vert i}$ and $u_{x,y\vert i}$ denote $\partial u_x/\partial x$ and $\partial u_x/\partial y$, respectively, evaluated at node i, with $i = 0$ for the centroid. The same shape functions interpolate $u_x(\zeta_1, \zeta_2, \zeta_3)$. The torsional mode with unit rotations $\theta_i = \bar{\theta} = 1$ is imposed by setting the nodal displacements to

$$u_{xi} = u_{yi} = u_{x,x\vert j} = u_{y,y\vert j} = 0, \quad u_{x,y\vert j} = -\bar{\theta}, \quad u_{y,x\vert j} = \bar{\theta}, \quad i = 0, 1, 2, 3, \ j = 1, 2, 3. \tag{88}$$

Differentiating the QST interpolation with respect to x and y, collapsing freedoms via (88) and transforming to natural strains via (11) yields

$$\epsilon_t = \begin{bmatrix} \epsilon_{t21} \\ \epsilon_{t32} \\ \epsilon_{t13} \end{bmatrix} = 3 \begin{bmatrix} \chi_{21\vert3}\,(\zeta_1 - \zeta_2)\zeta_3 \\ \chi_{32\vert1}\,(\zeta_2 - \zeta_3)\zeta_1 \\ \chi_{13\vert2}\,(\zeta_3 - \zeta_1)\zeta_2 \end{bmatrix} \bar{\theta}, \tag{89}$$

This quadratic field was found unable to produce optimal elements in conjunction with the foregoing bending field. A midpoint-filtered fit that permits optimality is obtained by collocating (89) at the midpoints and interpolating linearly over the triangle:

$$\epsilon_t^m = \begin{bmatrix} \epsilon_{t21}^m \\ \epsilon_{t32}^m \\ \epsilon_{t13}^m \end{bmatrix} = \tfrac{3}{2} \begin{bmatrix} \chi_{21\vert3}\,(\zeta_1 - \zeta_2) \\ \chi_{32\vert1}\,(\zeta_2 - \zeta_3) \\ \chi_{13\vert2}\,(\zeta_3 - \zeta_1) \end{bmatrix} \bar{\theta} \ \stackrel{\text{def}}{=} \ \frac{4A}{3}\psi_0 \begin{bmatrix} (\zeta_1 - \zeta_2)/\ell_{21}^2 \\ (\zeta_2 - \zeta_3)/\ell_{32}^2 \\ (\zeta_3 - \zeta_1)/\ell_{13}^2 \end{bmatrix} \bar{\theta}. \tag{90}$$

The effect of this strain filtering is pictured in Figure 23 using integrated displacement patterns.

As indicated on the right of (90) the field is scaled by a weight coefficient ψ_0 chosen so that $\psi_0 = 1$ for the parameter set that produces the optimal element. Evaluating (90) at corner 1, combining with (86) and using the rotational transformation (81) gives

$$\epsilon_1 = \frac{2A}{3} \begin{bmatrix} \frac{\psi_1}{\ell_{21}^2} & \frac{\psi_2}{\ell_{21}^2} & \frac{\psi_3}{\ell_{21}^2} & \frac{4\psi_0}{\ell_{21}^2} \\ \frac{\psi_4}{\ell_{32}^2} & \frac{\psi_5}{\ell_{32}^2} & \frac{\psi_6}{\ell_{32}^2} & 0 \\ \frac{\psi_7}{\ell_{13}^2} & \frac{\psi_8}{\ell_{13}^2} & \frac{\psi_9}{\ell_{13}^2} & \frac{-4\psi_0}{\ell_{13}^2} \end{bmatrix} \begin{bmatrix} \theta_1' \\ \theta_2' \\ \theta_3' \\ \bar{\theta} \end{bmatrix} = \frac{2A}{3} \begin{bmatrix} \frac{\beta_1}{\ell_{21}^2} & \frac{\beta_2}{\ell_{21}^2} & \frac{\beta_3}{\ell_{21}^2} \\ \frac{\beta_4}{\ell_{32}^2} & \frac{\beta_5}{\ell_{32}^2} & \frac{\beta_6}{\ell_{32}^2} \\ \frac{\beta_7}{\ell_{13}^2} & \frac{\beta_8}{\ell_{13}^2} & \frac{\beta_9}{\ell_{13}^2} \end{bmatrix} \begin{bmatrix} \tilde{\theta}_1 \\ \tilde{\theta}_2 \\ \tilde{\theta}_3 \end{bmatrix} = \mathbf{Q}_1\tilde{\boldsymbol{\theta}}, \tag{91}$$

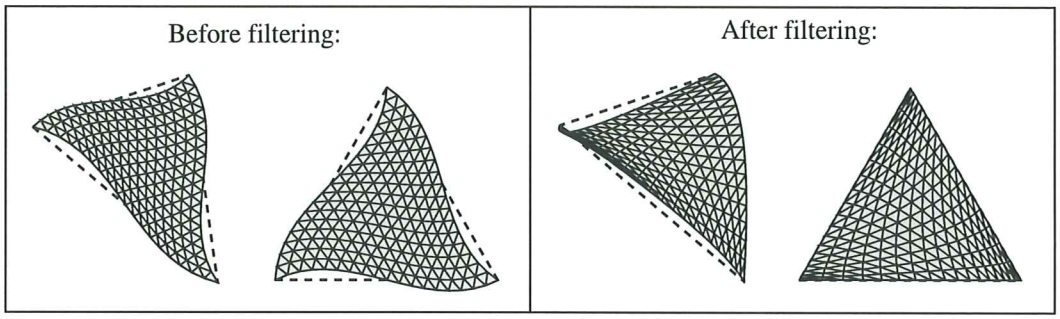

Figure 23. The torsional displacement mode before and after strain filtering. Filtered patterns were obtained by integrating the strain field (90). Note that for an equilateral triangle the filtered pattern becomes a bubble mode.

in which $\beta_1 = \frac{1}{3}(4\psi_0 + 2\psi_1 - \psi_2 - \psi_3)$, $\beta_2 = \frac{1}{3}(4\psi_0 - \psi_1 + 2\psi_2 - \psi_3)$, $\beta_3 = \frac{1}{3}(4\psi_0 - \psi_1 - \psi_2 + 2\psi_3)$, $\beta_4 = \frac{1}{3}(2\psi_4 - \psi_5 - \psi_6)$, $\beta_5 = \frac{1}{3}(-\psi_4 + 2\psi_5 - \psi_6)$, $\beta_6 = \frac{1}{3}(-\psi_4 - \psi_5 + 2\psi_6)$, $\beta_7 = \frac{1}{3}(-4\psi_0 + 2\psi_7 - \psi_8 - \psi_9)$, $\beta_8 = \frac{1}{3}(-4\psi_0 - \psi_7 + 2\psi_8 - \psi_9)$ and $\beta_9 = \frac{1}{3}(-4\psi_0 - \psi_7 - \psi_8 + 2\psi_9)$. Matrices $\mathbf{Q}_2$ and $\mathbf{Q}_3$ are obtained by cyclic permutation. These matrices are used in Section 4.6 to construct the ANDES template (31).

Appendix B. SOLVING POLYNOMIAL EQUATIONS FOR TEMPLATE OPTIMALITY

Let $\mathbf{p} = [\, p_1 \quad p_2 \quad \ldots \quad p_n \,]^T$ be a n-vector of template parameters. While seeking template optimality under high order patch tests one must usually deal with a polynomial energy ratio of the form

$$r(\mathbf{p}) = c_0 + c_2\gamma^2 + \ldots + c_k\gamma^k, \tag{92}$$

where k is even, γ is an element aspect ratio, and coefficients $c_j = c_j(\mathbf{p})$ for $j = 0, 2 \ldots k$, take on one of the quadratic forms

$$c_j = \mathbf{p}^T\mathbf{A}_j\mathbf{p}, \quad c_j = \mathbf{p}^T\mathbf{A}_j\mathbf{p} + 2\mathbf{b}_j^T\mathbf{p}, \quad \text{or} \quad c_j = \mathbf{p}^T\mathbf{A}_i\mathbf{p} + 2\mathbf{b}_j^T\mathbf{p} + d_j. \tag{93}$$

The *kernel matrices* $\mathbf{A}_j$, are $n \times n$ symmetric matrices whereas $\mathbf{b}_j$ is an n-vector. The second and third forms of (93) may be reduced to the homogeneous form by the obvious augmentation

$$\mathbf{p} \to \hat{\mathbf{p}} = [\, 1 \quad p_1 \quad p_2 \quad \ldots \quad p_k \,], \quad \mathbf{A}_j \to \hat{\mathbf{A}}_j = \begin{bmatrix} d_j & \mathbf{b}_j \\ \mathbf{b}_j^T & \mathbf{A}_j \end{bmatrix}, \quad c_j = \hat{\mathbf{p}}^T\hat{\mathbf{A}}_j\hat{\mathbf{p}}. \tag{94}$$

The optimization conditions are $c_0 = 1$ and $c_j = 0$ for $j = 2, \ldots k$. One is interested only in solutions $\mathbf{p} = [\, p_1 \quad \ldots \quad p_n \,]^T$ or $\hat{\mathbf{p}} = [\, 1 \quad \hat{p}_1 \quad \ldots \quad \hat{p}_n \,]^T$ with *real* entries. Preferably the solutions should be rational if the entries of $\mathbf{A}_j$, $\mathbf{b}_j$ and d_j are, as is often the case. If $n(k+2) > 4$, a brute force solution as a system of polynomial equations in exact rational aritmetic may be hopeless. It is observed in practice, however, that matrices $\mathbf{A}_j$ or $\hat{\mathbf{A}}_j$ are highly singular and nonnegative. This allows an efficient staged reduction scheme in which most of the steps involve only the solution of linear equations. The method will be explained by example, using the optimization of the ANDES template undertaken in Section 5 as case study.

The coefficients of the energy ratio r of (36)–(38): $r = c_0 + c_2\,\gamma^2 + c_4\,\gamma^4$ can be expressed as

$$c_0 - 1 = \mathbf{p}^T\mathbf{A}_0\mathbf{p}, \quad c_2 = \mathbf{p}^T\mathbf{A}_2\mathbf{p}, \quad c_4 = \mathbf{p}^T\mathbf{A}_4\mathbf{p}, \tag{95}$$

in which $\mathbf{p}$ is the 8-vector $[\, 1 \quad \alpha_b \quad \beta_1 \quad \beta_2 \quad \beta_3 \quad \beta_4 \quad \beta_5 \quad \beta_6 \,]$. This is actually the augmented vector denoted by $\hat{\mathbf{p}}$ above, with the hat suppressed for brevity, and likewise over the $\mathbf{A}_j$s. The kernel matrices are

$$\mathbf{A}_0 = \tfrac{1}{3}\begin{bmatrix} 9 & -3 & 0 & 0 & 0 & 0 & 0 & 0 \\ -3 & 1 & 0 & 0 & 0 & 0 & 0 & 0 \\ 0 & 0 & 0 & 0 & 0 & 0 & 0 & 0 \\ 0 & 0 & 0 & 0 & 0 & 0 & 0 & 0 \\ 0 & 0 & 0 & 0 & 0 & 0 & 0 & 0 \\ 0 & 0 & 0 & 0 & 0 & 0 & 0 & 0 \\ 0 & 0 & 0 & 0 & 0 & 0 & 0 & 0 \\ 0 & 0 & 0 & 0 & 0 & 0 & 0 & 0 \end{bmatrix} + \frac{\beta_0}{32}\begin{bmatrix} 0 & 0 & 0 & 0 & 0 & 0 & 0 & 0 \\ 0 & 0 & 0 & 0 & 0 & 0 & 0 & 0 \\ 0 & 0 & 13 & -11 & -1 & 2 & 2 & -6 \\ 0 & 0 & -11 & 13 & -1 & -2 & -2 & 6 \\ 0 & 0 & -1 & -1 & 1 & 0 & 0 & 0 \\ 0 & 0 & 2 & -2 & 0 & 1 & 1 & -3 \\ 0 & 0 & 2 & -2 & 0 & 1 & 1 & -3 \\ 0 & 0 & -6 & 6 & 0 & -3 & -3 & 9 \end{bmatrix}, \tag{96}$$

$$\mathbf{A}_2 = \tfrac{1}{6}\begin{bmatrix} -9 & -6 & 0 & 0 & 0 & 0 & 0 & 0 \\ -6 & 4 & 0 & 0 & 0 & 0 & 0 & 0 \\ 0 & 0 & 0 & 0 & 0 & 0 & 0 & 0 \\ 0 & 0 & 0 & 0 & 0 & 0 & 0 & 0 \\ 0 & 0 & 0 & 0 & 0 & 0 & 0 & 0 \\ 0 & 0 & 0 & 0 & 0 & 0 & 0 & 0 \\ 0 & 0 & 0 & 0 & 0 & 0 & 0 & 0 \\ 0 & 0 & 0 & 0 & 0 & 0 & 0 & 0 \end{bmatrix} + \frac{\beta_0}{32}\begin{bmatrix} 0 & 0 & 0 & 0 & 0 & 0 & 0 & 0 \\ 0 & 0 & 0 & 0 & 0 & 0 & 0 & 0 \\ 0 & 0 & 26 & -20 & -4 & -10 & 12 & -6 \\ 0 & 0 & -20 & 22 & -2 & 8 & -14 & 8 \\ 0 & 0 & -4 & -2 & 6 & 0 & 2 & 0 \\ 0 & 0 & -10 & 8 & 0 & 5 & -5 & 1 \\ 0 & 0 & 12 & -14 & 2 & -5 & 9 & -5 \\ 0 & 0 & -6 & 8 & 0 & 1 & -5 & 5 \end{bmatrix}, \tag{97}$$

$$\mathbf{A}_4 = \frac{\beta_0}{64}\begin{bmatrix} 0 & 0 & 0 & 0 & 0 & 0 & 0 & 0 \\ 0 & 0 & 0 & 0 & 0 & 0 & 0 & 0 \\ 0 & 0 & 1 & 1 & -3 & 0 & 0 & 0 \\ 0 & 0 & 1 & 1 & -3 & 0 & 0 & 0 \\ 0 & 0 & -3 & -3 & 9 & 0 & 0 & 0 \\ 0 & 0 & 0 & 0 & 0 & 9 & -3 & -3 \\ 0 & 0 & 0 & 0 & 0 & -3 & 1 & 1 \\ 0 & 0 & 0 & 0 & 0 & -3 & 1 & 1 \end{bmatrix} \tag{98}$$

The optimality conditions are $c_0 - 1 = 0$, $c_2 = 0$, $c_4 = 0$. Taking the higher order scaling factor $\beta_0 = 1/2$ for convenience, matrices $\mathbf{A}_0$, $\mathbf{A}_2$ and $\mathbf{A}_4$ have the eigenvalues

$$\begin{aligned} &\text{eigs of } \mathbf{A}_0\text{: [} 10/3 \quad 3/64 \quad (35+\sqrt{521})/128 \quad (35-\sqrt{521})/128 \quad 0 \quad 0 \quad 0 \quad 0 \text{]} \\ &\text{eigs of } \mathbf{A}_2\text{: [} 13/6 \quad 8053/8904 \quad 1063/6333 \quad 1774/25955 \quad 0 \quad 0 \quad 0 \quad 0 \text{]} \\ &\text{eigs of } \mathbf{A}_4\text{: [} 11/64 \quad 11/64 \quad 0 \quad 0 \quad 0 \quad 0 \quad 0 \quad 0 \quad 0 \quad 0 \text{]} \end{aligned} \tag{99}$$

(For $\mathbf{A}_2$ the listed eigenvalues #2 through #4 are rational approximants within 10^{-8}.) Consequently the conditions stated previously are met. Begin with $\mathbf{A}_4$, which has rank 2, rank deficiency 6, and spectral decomposition

$$\mathbf{A}_4 = \mathbf{V}_4\mathbf{\Lambda}_4\mathbf{V}_4^T, \quad \mathbf{\Lambda}_4 = \begin{bmatrix} \frac{11}{64} & 0 \\ 0 & \frac{11}{64} \end{bmatrix}, \quad \mathbf{V}_4 = \frac{1}{\sqrt{11}}\begin{bmatrix} 0 & 0 & -1 & -1 & 3 & 0 & 0 & 0 \\ 0 & 0 & 0 & 0 & 0 & -3 & 1 & 1 \end{bmatrix}^T. \tag{100}$$

Since $\mathbf{\Lambda}_4$ is positive definite the only real solutions of $c_4 = \mathbf{p}^T\mathbf{A}_4\mathbf{p} = \mathbf{p}^T\mathbf{V}_4\mathbf{\Lambda}_4\mathbf{V}_4^T\mathbf{p} = 0$ are those of $\mathbf{V}_4^T\mathbf{p} = \mathbf{0}$. This is an underdetermined *linear* system of 2 equations in 8 variables, from which 2 entries in $\mathbf{p}$ are designated as dependent and eliminated: $\beta_1 = 3\beta_3 - \beta_2$ and $3\beta_4 = \beta_5 + \beta_6$. Replacing these relations into $c_2 = \mathbf{p}^T\mathbf{A}_2\mathbf{p} = 0$ reduces $\mathbf{p}$ to six entries and $\mathbf{A}_2$ to 6×6. The reduced $\mathbf{A}_2$ is nonnegative definite and has rank 4. This allows 4 more variables to be eliminated. Repeating the spectral analysis yields $\alpha_b = 3/2$, $\beta_2 = -2\beta_6$, $\beta_3 = -\beta_6$ and $\beta_5 = -\beta_6$. Finally, replacing into $c_0 - 1 = 0$ gives $\beta_6^2 = 1$. Choosing $\beta_6 = -1$ the complete solution is

$$\alpha_b = \tfrac{3}{2}, \ \beta_0 = \tfrac{1}{2}, \ \beta_1 = \beta_3 = \beta_5 = 1, \ \beta_2 = 2, \beta_4 = 0, \ \beta_6 = \beta_7 = \beta_8 = -1, \ \beta_9 = -2, \tag{101}$$

which is used in Section 5.2.

It is not always necessary to do the complete eigenspectral analysis of the $\mathbf{A}_j$s. It is sufficient to get a full-rank basis $\mathbf{V}_j$ for the range spaces. This is easily done by getting the null space through the appropriate function of *Mathematica* or *Maple*, and then forming $\mathbf{V}$ as the orthogonal complement by Gram-Schmidt. This alternative path is useful for systems treated by exact arithmetic if the eigenvalues are complicated functions of the matrix coefficients.

Acknowledgements

The work reported here has been supported by Sandia National Labs under the Finite Elements for Salinas contract. Portions of the report were written while at CIMNE, Barcelona, Spain, under a fellowship granted by the Spanish Ministerio of Educación y Cultura.

References

[1] C. A. Felippa and C. Militello, Developments in variational methods for high performance plate and shell elements, in *Analytical and Computational Models for Shells*, CED Vol. 3, Eds. A. K. Noor, T. Belytschko and J. C. Simo, The American Society of Mechanical Engineers, ASME, New York, 1989, 191–216.

[2] R. H. MacNeal, The evolution of lower order plate and shell elements in MSC/NASTRAN, in T. J. R. Hughes and E. Hinton (eds.), *Finite Element Methods for Plate and Shell Structures, Vol. I: Element Technology*, Pineridge Press, Swansea, U.K., 1986, 85–127.

[3] C. A. Felippa, Introduction to Finite Element Methods course, `http:caswww.colorado.edu/courses.d/IFEM.d/Home.html`

[4] K. Alvin, H. M. de la Fuente, B. Haugen and C. A. Felippa, Membrane triangles with corner drilling freedoms: I. The EFF element, *Finite Elements Anal. Des.*, **12**, 163–187, 1992.

[5] V. Boltyanskii, R. Gamkrelidze and L. Pontryagin, On the theory of optimal processes, *Rep. Acam. Sci. USSR, 110*, 1956, 7–10.

[6] R. Bellman, *Adaptive Control Processes: A Guided Tour*, Princeton Univ. Press, 1961.

[7] C. A. Felippa, Recent advances in finite element templates, Chapter 4 in *Computational Mechanics for the Twenty-First Century*, ed. by B.H.V. Topping, Saxe-Coburn Publications, Edinburgh, 71–98, 2000.

[8] R. W. Clough, The finite element method – a personal view of its original formulation, in *From Finite Elements to the Troll Platform - the Ivar Holand 70th Anniversary Volume*, ed. by K. Bell, Tapir, Trondheim, Norway, 89–100, 1994.

[9] M. J. Turner, R. W. Clough, H. C. Martin, and L. J. Topp, Stiffness and deflection analysis of complex structures, *J. Aero. Sci.*, **23**, pp. 805–824, 1956.

[10] O. C. Zienkiewicz, personal communication, Barcelona, May 2001.

[11] B. M. Fraeijs de Veubeke, Displacement and equilibrium models, in *Stress Analysis*, ed. by O. C. Zienkiewicz and G. Hollister, Wiley, London, 1965, 145–197. Reprinted in *Int. J. Numer. Meth. Engrg.*, **52**, 287–342, 2001.

[12] C. A. Felippa, Refined finite element analysis of linear and nonlinear two-dimensional structures, *Ph.D. Dissertation*, Department of Civil Engineering, University of California at Berkeley, Berkeley, CA, 1966.

[13] G. P. Bazeley, Y. K. Cheung, B. M. Irons and O. C. Zienkiewicz, Triangular elements in plate bending – conforming and nonconforming solutions, in *Proc. 1st Conf. Matrix Meth. Struc. Mech.*, ed. by J. Przemieniecki et. al., AFFDL-TR-66-80, Air Force Institute of Technology, Dayton, Ohio, 1966, 547–576.

[14] A. J. Carr, A refined finite element analysis of thin shell structures including dynamic loadings, *Ph. D. Dissertation*, Department of Civil Engineering, University of California at Berkeley, Berkeley, CA, 1968.

[15] R. W. Clough, Analysis of structural vibrations and dynamic response, in *Recent Advances in Matrix Methods of Structural Analysis and Design*, ed by R. H. Gallagher, Y. Yamada and J. T. Oden, University of Alabama Press, Hunstsville, AL, 1971, 441–486.

[16] B. N. Abu-Gazaleh, Analysis of plate-type prismatic structures, *Ph. D. Dissertation*, Dept. of Civil Engineering, Univ. of California, Berkeley, CA, 1965.

[17] K. J. Willam, Finite element analysis of cellular structures, *Ph. D. Dissertation*, Dept. of Civil Engineering, Univ. of California, Berkeley, CA, 1969.

[18] C. C. Rankin, F. A. Brogan, W. A. Loden and H. Cabiness, *STAGS User Manual*, Lockheed Mechanics, Materials and Structures Report P032594, Version 3.0, January 1998.

[19] C. A. Felippa and C. Militello, Membrane triangles with corner drilling freedoms: II. The ANDES element, *Finite Elements Anal. Des.*, **12**, 189–201, 1992.

[20] C. A. Felippa and S. Alexander, Membrane triangles with corner drilling freedoms: III. Implementation and performance evaluation, *Finite Elements Anal. Des.*, **12**, 203–239, 1992.

[21] P. G. Bergan, Finite elements based on energy orthogonal functions, *Int. J. Numer. Meth. Engrg.*, **15**, 1141–1555, 1980.

[22] P. G. Bergan and M. K. Nygård, Finite elements with increased freedom in choosing shape functions, *Int. J. Numer. Meth. Engrg.*, **20**, 643–664, 1984.

[23] P. G. Bergan and C. A. Felippa, A triangular membrane element with rotational degrees of freedom, *Comp. Meths. Appl. Mech. Engrg.*, **50**, 25–69, 1985.

[24] P. G. Bergan and C. A. Felippa, Efficient implementation of a triangular membrane element with drilling freedoms, in T. J. R. Hughes and E. Hinton (eds.), *Finite Element Methods for Plate and Shell Structures, Vol. I: Element Technology*, Pineridge Press, Swansea, U.K., 1986, 128–152.

[25] M. K. Nygård, The Free Formulation for nonlinear finite elements with applications to shells, *Ph. D. Dissertation*, Division of Structural Mechanics, NTH, Trondheim, Norway, 1986.

[26] C. A. Felippa and P. Bergan, A triangular plate bending element based on an energy-orthogonal free formulation, *Comp. Meths. Appl. Mech. Engrg.*, **61**, 129–160, 1987.

[27] C. A. Felippa, Parametrized multifield variational principles in elasticity: II. Hybrid functionals and the free formulation, *Comm. Appl. Numer. Meth.*, **5**, 79–88, 1989.

[28] C. A. Felippa, The extended free formulation of finite elements in linear elasticity, *J. Appl. Mech.*, **56**, 609–616, 1989.

[29] G. Skeie, The Free Formulation: linear theory and extensions with applications to tetrahedral elements with rotational freedoms, *Ph. D. Dissertation*, Division of Structural Mechanics, NTH, Trondheim, Norway, 1991.

[30] K. C. Park and G. M. Stanley, A curved C^0 shell element based on assumed natural-coordinate strains, *J. Appl. Mech.*, **53**, 278–290, 1986.

[31] G. M. Stanley, K. C. Park and T. J. R. Hughes, Continuum based resultant shell elements, in T. J. R. Hughes and E. Hinton (eds.), *Finite Element Methods for Plate and Shell Structures, Vol. I: Element Technology*, Pineridge Press, Swansea, U.K., 1986, 1–45.

[32] C. Militello, Application of parametrized variational principles to the finite element method, *Ph. D. Dissertation*, Department of Aerospace Engineering Sciences, University of Colorado, Boulder, CO, 1991.

[33] C. Militello and C. A. Felippa, The first ANDES elements: 9-DOF plate bending triangles, *Comp. Meths. Appl. Mech. Engrg.*, **93**, 217–246. 1991.

[34] P. G. Bergan and L. Hanssen, A new approach for deriving 'good' finite elements, MAFELAP II Conference, Brunel University, 1975, in *The Mathematics of Finite Elements and Applications – Volume II*, ed. by J. R. Whiteman, Academic Press, London, 483–497, 1976.

[35] T. Belytschko, W. K. Liu and B. E. Engelmann, The gamma elements and related developments, in T. J. R. Hughes and E. Hinton (eds.), *Finite Element Methods for Plate and Shell Structures, Vol. I: Element Technology*, Pineridge Press, Swansea, U.K., 316–347, 1986.

[36] T. J. R. Hughes, *The Finite Element Method: Linear Static and Dynamic Finite Element Analysis*, Prentice Hall, Englewood Cliffs, N. J., 1987.

[37] C. Militello and C. A. Felippa, The individual element patch revisited, in *The Finite Element Method in the 1990's — a book dedicated to O. C. Zienkiewicz*, ed. by E. Oñate, J. Periaux and A. Samuelsson, CIMNE, Barcelona and Springer-Verlag, Berlin, 554–564, 1991.

[38] C. A. Felippa, A survey of parametrized variational principles and applications to computational mechanics, *Comp. Meths. Appl. Mech. Engrg.*, **113**, 109–139, 1994.

[39] C. A. Felippa, B. Haugen and C. Militello, From the individual element test to finite element templates: evolution of the patch test, *Int. J. Numer. Meth. Engrg.*, **38**, 199–229, 1995.

[40] C. A. Felippa and C. Militello, Construction of optimal 3-node plate bending elements by templates, *Comput. Mech.*, **24/1**, 1–13, 1999.

[41] C. A. Felippa, Recent developments in basic finite element technologies, in *Computational Mechanics in Structural Engineering - Recent Developments*, ed. by F. Y. Cheng and Y. Gu, Elsevier, Amsterdam, 141–156, 1999.

[42] C. A. Felippa, Customizing the mass and geometric stiffness of plane thin beam elements by Fourier methods, *Engrg. Comput.*, **18**, 286–303, 2001.

[43] C. A. Felippa, Customizing high performance elements by Fourier methods, *Trends in Computational Mechanics*, ed. by W. A. Wall, K.-U. Bleitzinger and K. Schweizerhof, CIMNE, Barcelona, Spain, 283-296, 2001.

[44] Przemieniecki, J. S., *Theory of Matrix Structural Analysis*, McGraw-Hill, New York, 1968; Dover edition 1986.

[45] B. M. Irons and S. Ahmad, *Techniques of Finite Elements*, Ellis Horwood Ltd, 1980.

[46] C. A. Felippa and R. W. Clough, The finite element method in solid mechanics, in *Numerical Solution of Field Problems in Continuum Physics*, ed. by G. Birkhoff and R. S. Varga, SIAM–AMS Proceedings II, American Mathematical Society, Providence, R.I., 210–252, 1969.

[47] D. J. Allman, A compatible triangular element including vertex rotations for plane elasticity analysis, *Computers & Structures*, **19**, 1–8, 1984.

[48] D. J. Allman, Evaluation of the constant strain triangle with drilling rotations, *Int. J. Numer. Meth. Engrg.*, **26**, 2645–2655, 1988.

[49] R. D. Cook, Improved two-dimensional finite element, *Journal of the Structural Division*, ASCE, **100**, ST6, pp. 1851–1863, 1974.

[50] J. Wimp, *Sequence Transformations and Their Applications*, Academic Press, New York, 1981.

[51] R. L. Taylor, P. J. Beresford and E. L. Wilson, A non-conforming element for stress analysis, *Int. J. Numer. Meth. Engrg.*, **10**, pp. 1211–1219, 1976.

[52] R. D. Cook, Ways to improve the bending response of finite elements, *Int. J. Numer. Meth. Engrg.*, **11**, pp. 1029–1039, 1977.

[53] C. Farhat, P. Geuzaine and G. Brown, Application of a three-field nonlinear fluid-structure formulation to the prediction of the aeroelastic parameters of an F-16 fighter, *Computers and Fluids*, in press.

[54] B. Haugen, Buckling and stability problems for thin shell structures using high-performance finite elements, *Ph. D. Dissertation*, Dept. of Aerospace Engineering Sciences, University of Colorado, Boulder, CO, 1994.